JOC The Journal of Organic Chemistry

Article

adj-Dicarbaporphyrinoid Systems: Synthesis, Spectroscopic Characterization and Reactivity of 23-Carbabenziporphyrins

Pankaj Jain, Deyaa I. AbuSalim, and Timothy D. Lash

J. Org. Chem., **Just Accepted Manuscript** • DOI: 10.1021/acs.joc.9b01410 • Publication Date (Web): 23 Jul 2019

Just Accepted

is published by the American Chemical Society. 1155 Sixteenth Street N.W., Washington, DC 20036

adj-Dicarbaporphyrinoid Systems: Synthesis, Spectroscopic Characterization and Reactivity of 23-Carbabenziporphyrins

Pankaj Jain, Deyaa I. AbuSalim and Timothy D. Lash*

Department of Chemistry, Illinois State University, Normal, Illinois 61790-4160

E-mail: tdlash@ilstu.edu

Abstract

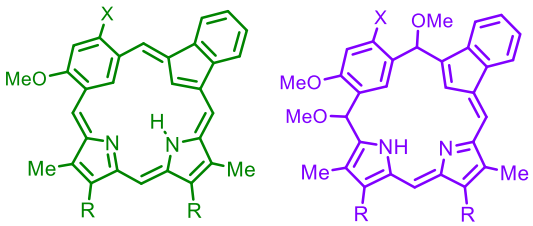

X = H or OMe
R = Et, Me or $CH_2CH_2CO_2Me$

A new family of *adj*-dicarbaporphyrinoids has been prepared using the '2 + 2' MacDonald methodology. Dibutylboron triflate catalyzed condensation of 3-iodo-4-methoxy-benzaldehyde with an indene enamine afforded an iodofulvene aldehyde, and a related dimethoxyfulvene was similarly prepared in two steps from 2,4-dimethoxybenzaldehyde. Following protection as the corresponding dimethyl acetals, the iodofulvenes were metalated with Bu_3MgLi at -100 ^oC and reacted with DMF to give the required fulvene dialdehyde intermediates. Acid-catalyzed condensation with three different dipyrrylmethanes afforded a series of benzo-23-carbabenziporphyrins in 52-70% yields. The proton NMR spectra for these *adj*-dicarbaporphyrinoids indicate that these macrocycles are slightly diatropic. Monoprotonation afforded cationic species with slightly larger aromatic ring currents, and under strongly acidic conditions C-protonated dications were generated with substantial diatropic properties. The aromatic character of these structures was supported by nucleus independent chemical shifts and anisotropy of induced current density calculations. The computational results indicate that the dications favor 23-atom 22π electron delocalization pathways. The benzo-23-carbabenziporphyrins were selectively oxidized with silver(I) acetate in dichloromethane-methanol to give stable nonaromatic structures with two additional methoxy-substituents

connected to sp^3 hybridized bridging carbons. The intriguing reactivity and unique spectroscopic properties of benzo-23-carbabenziporphyrins makes these novel structures promising candidates for further investigations.

Introduction

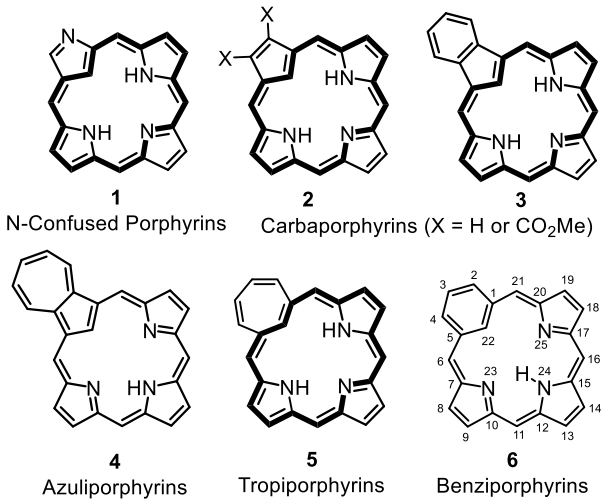

Figure 1. Selected carbaporphyrinoid systems.

Carbaporphyrinoid systems are an important group of porphyrin analogues that have been widely investigated over the last two decades due to their unusual reactivity and intriguing spectroscopic properties.[1] They include N-confused porphyrins **1**,[2,3] true carbaporphyrins such as **2** and **3**,[4-6] azuliporphyrins **4**,[7] tropiporphyrins **5**[8] and benziporphyrins **6** (Figure 1).[9] Each of these families can generate stable organometallic derivatives[10] and often undergo regioselective oxidation reactions.[1] Although **1**-**3** exhibit strongly aromatic characteristics, benziporphyrins are essentially nonaromatic while azuliporphyrins have intermediary aromatic properties. However, benziporphyrins take on a degree of diatropic character when electron-donating methoxy-groups are present (e.g. structure **7**)[11,12] and this is intensified upon protonation (Figure 2). The aromatic character of **7** can be attributed to contributions from dipolar canonical forms such as **7'** or π-delocalized structures such as **7''** that incorporate an 18π electron anionic diaza[17]annulene

pathway, but these interactions are limited because of the necessity for charge separation.[13] Addition of acid affords diprotonated dications **7**H_2^{2+} that exhibit substantial diatropic character. This can be explained by the presence of resonance contributors such as **7'**H_2^{2+} that facilitate charge delocalization or by contributions from species such as **7''**H_2^{2+} with cationic [19]annulene pathways.[11-13]

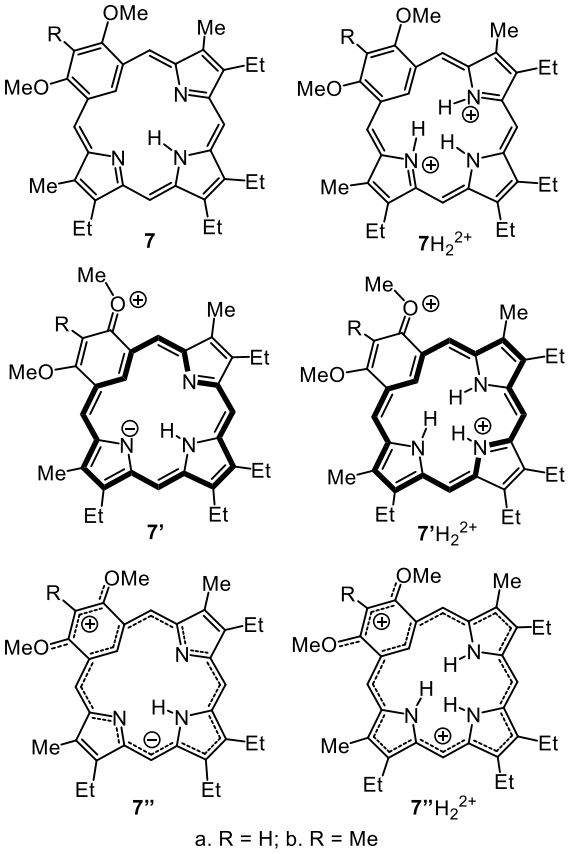

Figure 2. Conjugation pathways in free base and protonated dimethoxybenziporphyrins.

Dicarbaporphyrinoid systems, which have two carbon atoms within the macrocyclic core, are less well explored but a substantial number of examples have now been reported including doubly N-confused porphyrins,[14] *opp*- and *adj*-dicarbaporphyrins,[15,16] dioxadicarbaporphyrins,[17] dicarbachlorins,[18] *adj*-diazuliporphyrins,[19] hetero-*opp*-diazuliporphyrins,[20] dibenziporphyrins,[21] 22- and 23-carbaazuliporphyrins,[22,23] and 23-carbaoxybenziporphyrins.[24] In addition, a

dicarbacorrole system **8** called phenanthriporphyrin has been described (Figure 3),[25,26] and related dimeric structures have been investigated.[27] Dicarbaporphyrinoids may exhibit aromatic, nonaromatic or antiaromatic characteristics and can stabilize transition metal ions in high oxidation states such as copper(III). Regioselective oxidation reactions have also been observed and 22-carbaazuliporphyrins **9** were found to react with silver(I) acetate in the presence of methanol or ethanol to give the nonaromatic dialkoxy derivatives **10** (Figure 3). Although only one diastereomer was observed, the identity of this species (*cis*- or *trans*-) could not be identified. Similar reactivity was recently reported for reactions of phenanthriporphyrin **8** with copper(II) acetate in chloroform-methanol, but in this case the product **11** was generated as a mixture of *cis*- and *trans*-isomers.[26]

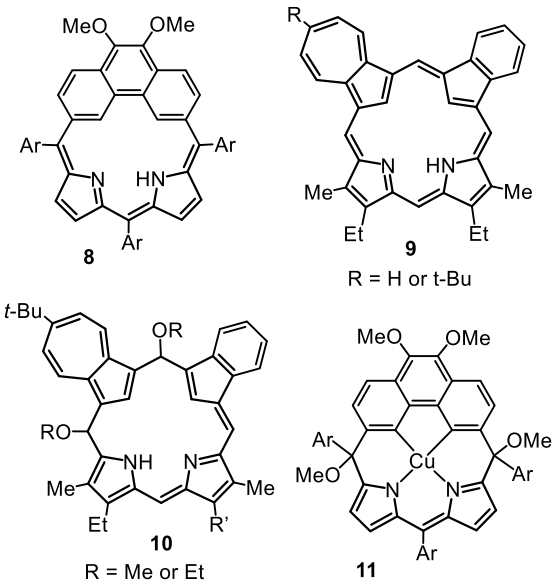

Figure 3. Dicarbaporphyrinoids and their oxidation products.

The interesting properties and potential applications associated with dicarbaporphyrinoids provide the incentive to further investigate structures of this type. Given the intermediary macrocyclic aromaticity associated with methoxybenziporphyrins, it was of interest to explore the properties of dicarba-analogues. In particular, methoxy- and dimethoxy-23-

carbabenziporphyrins **12** (Scheme 1) were targeted for synthesis. It was anticipated that the desired dicarbaporphyrinoids could be constructed using a '2 + 2' MacDonald condensation[28] from fulvene dialdehydes **13** and **14** and the known dipyrrylmethanes **15**.[29] The design and implementation of efficient syntheses of **12** are described below and the aromatic properties of these novel macrocycles, both as the free bases and in protonated form, were assessed by proton NMR spectroscopy and DFT calculations. Although metalation of these porphyrinoids was not accomplished, regioselective oxidation reactions were observed.

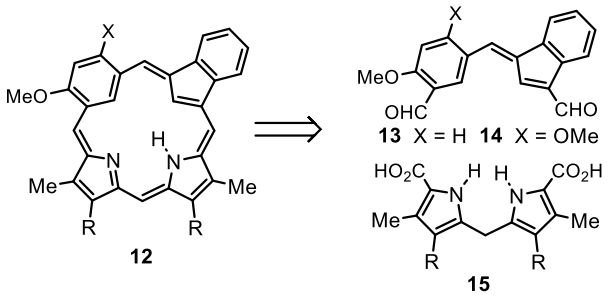

Scheme 1. Retrosynthetic analysis of 23-carbabenziporphyrins

Results and Discussion

Synthesis and Spectroscopic Characterization of 23-Carbabenziporphyrins

The synthesis of 23-carbabenziporphyrins **12** necessitated access to fulvene dialdehyde intermediates (Scheme 1). In earlier work, a synthesis of fulvene aldehydes was developed using indene enamine **16** (Scheme 2).[30] Reaction of **16** with aromatic aldehydes in the presence of dibutylboron triflate, followed by hydrolysis with aqueous sodium acetate, afforded good yields of structurally diverse monoaldehydes **17**. The main challenge at this point was the introduction of a second formyl moiety. Attempts to generate fulvene dialdehydes by reacting isophthalaldehydes **18** with one equivalent of **16** and Bu_2BOTf were unsuccessful and only difulvenes **19** could be isolated.[31,32] Reaction of a monocyanovinyl protected isophthalaldehyde **20** with **16** gave good yields of fulvene **21** but attempts to cleave the cyanovinyl group with

refluxing aqueous sodium hydroxide led to decomposition. Benzaldehydes **22** with vinyl or cyano groups that could conceivably be converted into formyl units were also reacted with **16** and Bu_2BOTf, but these reactions primarily led to decomposition and no fulvene products could be isolated. All of the alternative Lewis acid catalysts that had been investigated gave poor results and produced virtually none of the required fulvene aldehydes in any of these reactions.[31]

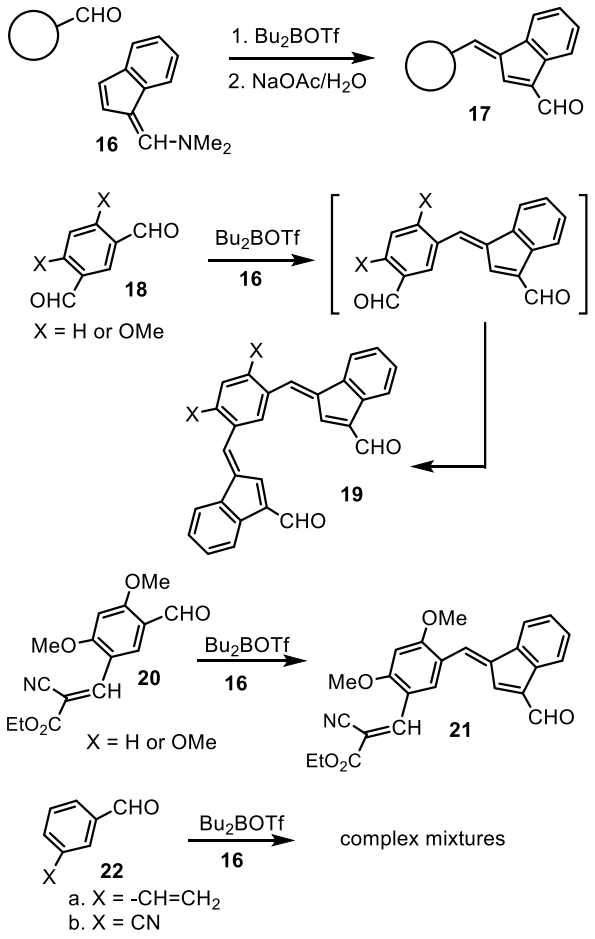

Scheme 2. Unsuccessful routes to fulvene dialdehydes.

Given these difficulties, an alternative strategy involving metal-halogen exchange had to be developed. Initial efforts were directed towards the synthesis of monomethoxyfulvene **13**. 3-Bromo-4-methoxybenzaldehyde (**23a**) was reacted with **16**[30] and Bu_2BOTf in dichloromethane, and hydrolyzed with aqueous sodium acetate, to give bromofulvene **24a** in 62% yield (Scheme

3). In order to install a second formyl moiety, it was necessary to protect and metalate the structure. Reaction of **24a** with trimethyl orthoformate and cerium(III) chloride afforded the corresponding acetal **25a** but reaction with *n*-butyllithium or *tert*-butyllithium failed to promote metal-halogen exchange. In order to increase the reactivity towards metalation, the analogous iodofulvene **24b** was prepared. Reaction of 3-iodo-4-methoxybenzaldehyde (**25b**)[33] with enamine **16** afforded fulvene **24b** in 43% yield. Protection with $CH(OMe)_3$-$CeCl_3$ gave the related acetal **25b** in 87% yield and this was treated with *n*-butyllithium in an attempt to generate the lithiated derivative. Unfortunately, no reaction was observed under any of the conditions investigated.

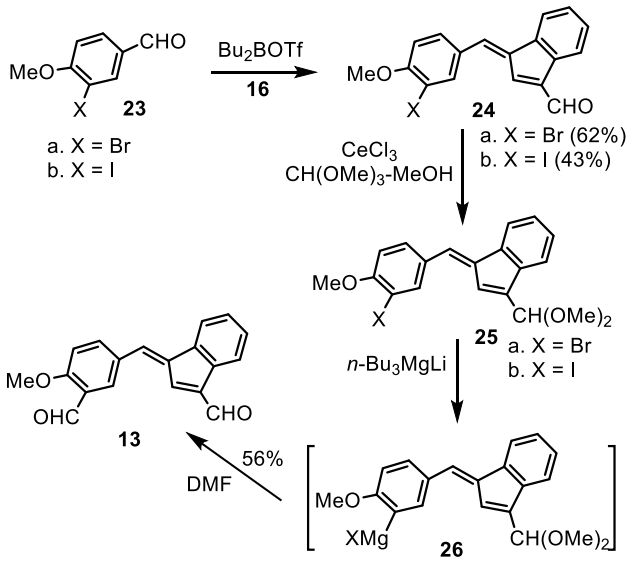

Scheme 3. Synthesis of a methoxyfulvene dialdehyde.

As magnesium ate complexes are known to increase reactivity in metal-halogen exchange reactions,[34-40] halogen-magnesium exchange was investigated for fulvene derivatives **25a** and **25b**. Tributylmagnesium-ate complex *n*-Bu_3MgLi is commonly used in these reactions and this

can be prepared by reacting 2 equivalents of a 1.6 M solution of *n*-butyllithium in hexanes with a 2.0 M solution of *n*-butylmagnesium chloride in THF in ether at 0 °C. Metal-halogen exchange is favored at very low temperatures and the temperature of the reactants was lowered to -100 °C. Although protected bromofulvene **25a** still failed to react, iodofulvene **25b** reacted with Bu_3MgLi in anhydrous ether at -100°C to give a metalated species **26** that reacted with DMF to afford dialdehyde **13** in 56% yield (Scheme 3).

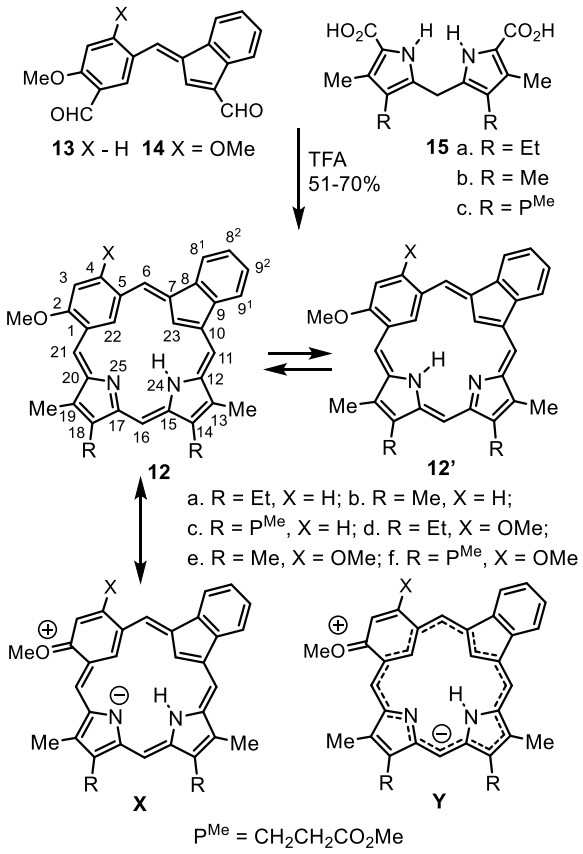

Scheme 4. Synthesis of 23-carbabenziporphyrins.

Fulvene dialdehyde **13** was reacted with dipyrrylmethane dicarboxylic acid **15a** and TFA in dichloromethane. Following column chromatography on silica gel and recrystallization from chloroform-hexanes, excellent yields (65-70%) of methoxycarbabenziporphyrin **12a** were obtained (Scheme 4). This is the first example of a fully conjugated *adj*-dicarbaporphyrinoid

incorporating a benzene subunit. The spectroscopic properties for dicarbaporphyrin **12a** indicate that it is a non-aromatic compound due to the presence of a cross-conjugated benzene subunit, although the proton NMR spectrum for this compound suggests that a weak macrocyclic ring current is present. Two tautomers of this system, **12** and **12'**, are conceivable, but only one species is observed in the proton NMR spectrum, possibly due to rapid exchange of the NH proton. The proton NMR spectrum of the free base (Figure 4A) showed four singlets corresponding to the *meso*-protons at 6.53, 7.01, 7.87 and 7.90 ppm, the inner benzene C-H appeared at 6.02 ppm, and the inner indene showed up at 4.97 ppm. The slight upfield shifts to the internal proton resonances, and the relatively deshielded values observed for the external protons, suggest that the macrocycle possesses a small amount of global diatropic character that presumably results from dipolar resonance contributors such as **X** or delocalized species such as **Y** with a 17-atom 18π electron delocalization pathway (Scheme 4). These properties are magnified upon addition of trace amounts of TFA to the NMR solution as the resulting monocation **12a**H^+ (Scheme 5) exhibits a significant, albeit modest, aromatic ring current. However, the precise values for these resonances depended on the concentration of TFA in the NMR tube (Figures 4B-G). The interior indene and benzene protons shifted upfield to ca. 4.5 ppm, while the exterior *meso*-proton resonances gave rise to four downfield singlets between 6.8 and 8.20 ppm. Furthermore, the methyl substituents shifted downfield from 2.49 ppm in the free base to >2.6 ppm in the monoprotonated structure. The emergence of an enhanced diatropic ring current can be attributed to resonance contributors such as **12**$^{\mathbf{R}}H^+$ that possess [18]annulene delocalization pathways (Figure 5). Contributors of this type would provide beneficial charge delocalization in addition to aromatic characteristics.

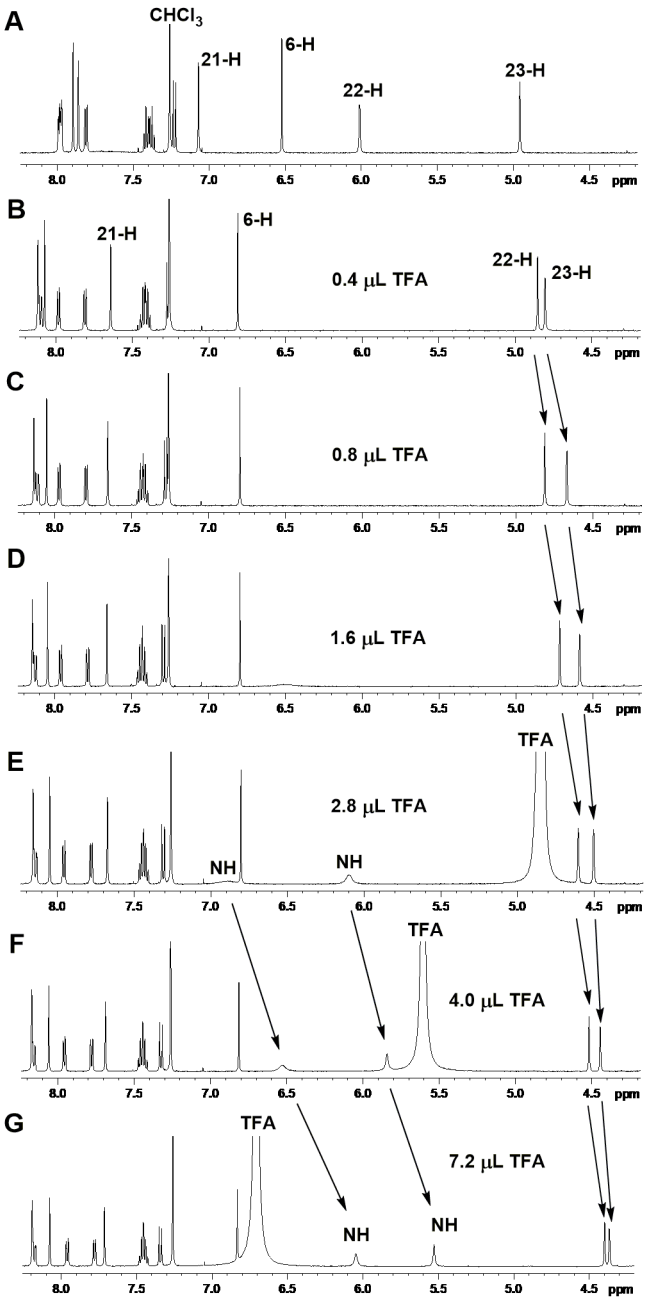

Figure 4. Proton NMR spectra of methoxy-23-carbabenziporphyrin **12a** (ca. 1.5 mg) in $CDCl_3$ (**A**, free base) and with incremental quantities of TFA (**B-G**, monocation **12a**H^+).

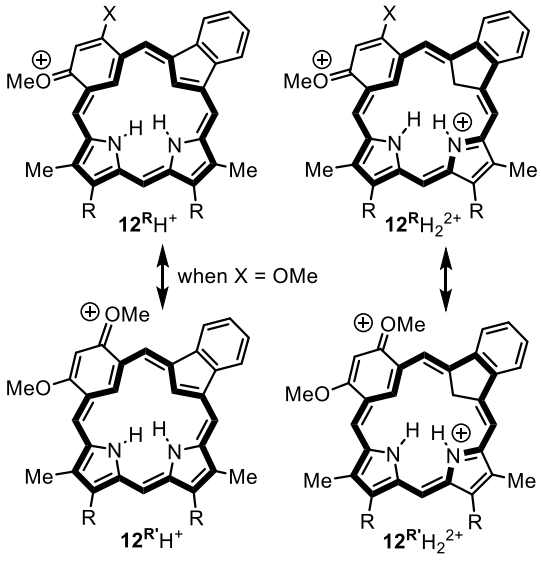

Figure 5. Canonical forms of protonated 23-carbabenziporphyrins **12** possessing 18π electron delocalization pathways.

The formation of monocation **12a**H^+ was examined by adding small increments of TFA to an NMR solution of ca. 1.5 mg of **12** (Figure 4). The internal proton on the benzene unit shifted upfield from 6.02 ppm to 4.80 ppm when 0.4 μL of TFA was added, and eventually overlapped with the internal indene proton at 4.35 ppm upon addition of 11.2 μL of TFA. At low concentrations of TFA, the NH resonances could not be discerned but an NH peak could be identified when 1.6 μL of TFA was added and a second NH peak became visible with 2.8 μL of TFA. Two NH resonances gave clear singlets when 4.0 μL of TFA was added and continued to move further upfield as the concentration of TFA was further increased. Although the changes observed for the downfield protons were much smaller, further downfield shifts were noted as the concentration of TFA increased (Figure 4). Profound changes to the electronic characteristics due to the protonation of dicarbaporphyrin **12a** can also be seen in the UV-vis spectra (Figure 6). The free base gave Soret-like bands at 352 and 415 nm and a broad absorption between 500 and 750 nm (Figure 6). Titration of **12a** with TFA showed the gradual transformation to a new

species that was attributed to monocation **12a**H^+ (Figure 7). Isosbestic points were observed at 375 and 445 nm, indicating that no significant concentrations of any other species are present in solution. The Soret-type band at 352 nm became more intense, while the band at 415 nm virtually disappeared upon addition of 20 equiv of TFA (Figure 7). The longer wavelength region between 450 and 800 nm showed Q-type bands more consistent with an aromatic porphyrinoid. In 100% TFA, the porphyrinoid gave a completely different UV-vis spectrum due to the formation of dication **12a**H_2^{2+}. This species shows a strong Soret-like band at 395 nm and moderately strong absorptions at 482 and 674 nm (Figure 6).

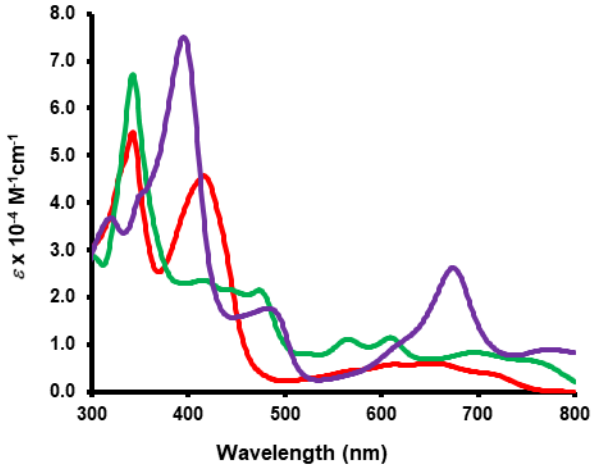

Figure 6. UV-vis spectra of **12a** in 1% triethylamine-chloroform (free base, red line), 1% TFA-chloroform (monocation **12a**H^+, green line) and 100% TFA (dication **12a**H_2^{2+}, purple line).

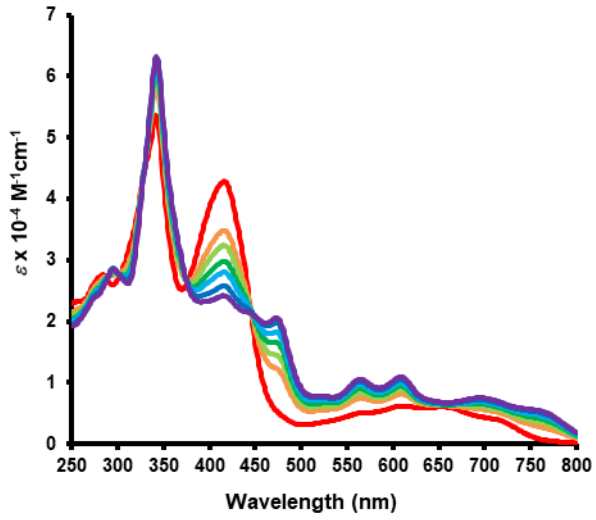

Figure 7. UV-vis spectra of **12a** in chloroform with incremental quantities of TFA: 0 equiv (red line), 1 equiv (orange) 2 equiv (light green), 3 equiv (dark green), 5 equiv (light blue), 10 equiv (dark blue) and 20 equiv (purple).

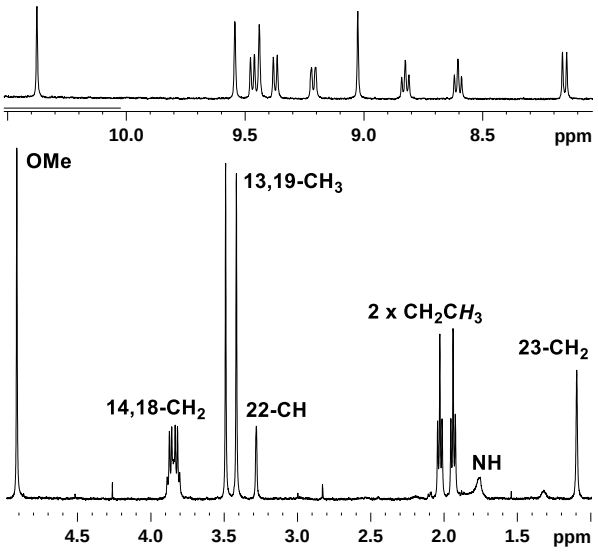

Figure 8. 500 MHz proton NMR spectrum of methoxy-23-carbabenziporphyrin dication **12a**H_2^{2+} in neat TFA.

The proton NMR spectrum of **12a**H_2^{2+} in 100% TFA confirmed that the macrocycle had undergone C-protonation onto the internal indene carbon atom and demonstrated that the dication exhibited a much larger diamagnetic ring current (Figure 8). The *meso*-protons showed

up as four 1H singlets at 9.04, 9.45, 9.55 and 10.31 ppm, while the internal benzene proton moved upfield to 3.29 ppm and the internal methylene unit gave a 2H singlet at 1.11 ppm. The methyl protons were observed at 3.43 and 3.50 ppm, shifted downfield by approximately 1 ppm compared to the free base. Although the positive charges may play a role in the downfield shifts, the observed differences in the chemical shifts for the internal and external sp^2 hybridized CHs ($\Delta\delta$ = 7.02 ppm) can only be explained by the presence of a strong aromatic ring current. The aromatic character of **12a**H_2^{2+} can again be attributed to electron-donation from the methoxy substituent as this facilitates canonical forms such as **12a^{R}**H_2^{2+} with 18π electron delocalization pathways (Figure 5). The ^{1}H-^{1}H COSY NMR spectrum for **12a**H_2^{2+} showed a weak correlation between the internal CH_2 and the nearby *meso*-protons (^4J or allylic coupling), but this interaction did not resolve in the proton NMR spectrum and only resulted in a slight broadening of these resonances. When the proton NMR spectrum of **12a** was run in 100% *d*-TFA, the internal NH and indene protons, and the *meso*-proton at position 16, were completely exchanged. These results indicate that dication **12a**H_2^{2+} must be in equilibrium with a *meso*-protonated dication **12a'**H_2^{2+} or the related monocations **12a'**H^+ and **12a''**H^+ (Scheme 5).

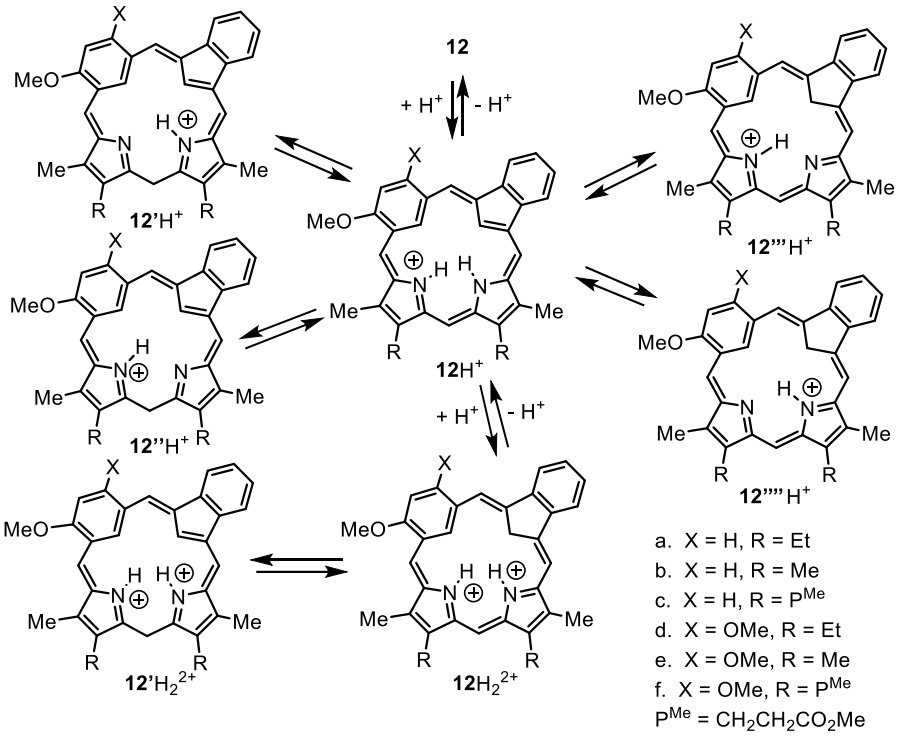

Scheme 5. Protonation of benzo-23-carbabenziporphyrins.

Fulvene dialdehyde **13** was also reacted with dipyrrylmethanes **15b** and **15c** to give the related methoxycarbabenziporphyrins **12b** and **12c** in 68% and 63% yields, respectively (Scheme 4). The spectroscopic properties of these porphyrinoids were very similar to those for **12a**, although **12b** was insufficiently soluble in organic solvents to allow a carbon-13 NMR spectrum to be obtained for the free base structure.

In order to magnify the aromatic characteristics of 23-carbabenziporphyrins, related structures with two methoxy-substituents (i.e. **12d-f**) were targeted for synthesis. Using the same synthetic strategy required the availability of 3-iodo-2,4-dimethoxybenzaldehyde (**27**), and this precursor was prepared by reacting 2,4-dimethoxybenzaldehyde with iodine and periodic acid in presence of sulfuric acid and acetic acid (Scheme 6).[33] However, when **27** was reacted with indene enamine **16** in the presence of Bu_2BOTf, fulvene **28** was generated instead of the required iodo-derivative. The loss of the iodo-substituent under these reaction conditions was attributed to the

electron-rich nature of the aryl unit, which can facilitate protonation-deiodination. Hence, a slightly different approach was used where the iodination was carried out after the fulvene had been formed. 2,4-Dimethoxybenzaldehyde was reacted with indene enamine **16** to afford fulvene **28**, and subsequent iodination with *N*-iodosuccinimide in the presence of catalytic TFA gave the required iodofulvene **29**. The product was contaminated with 3-5% of a second unidentified species that could not be removed by column chromatography. The iodo-compound was taken on in crude form and the aldehyde unit protected as dimethyl acetal **30** with $CH(OMe)_3$-$CeCl_3$. Iodine-magnesium exchange was carried out in the presence of the magnesium ate complex Bu_3MgLi at -100 °C, and subsequent addition of DMF and acid-catalyzed hydrolysis gave the dialdehyde **14** in 70% yield (56% from monoaldehyde **29**). Again, this intermediate was contaminated with a small amount of a second species that could not be removed. Nevertheless, this material proved to be a suitable precursor in the synthesis of the targeted dimethoxyporphyrinoids **12d-f**.

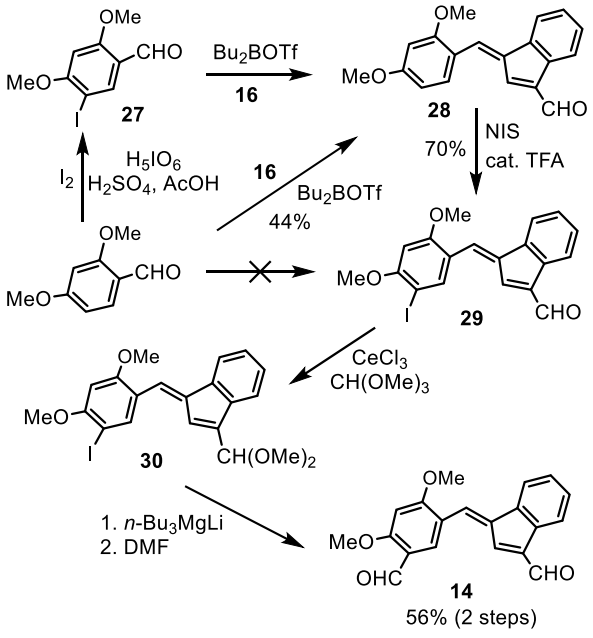

Scheme 6. Synthesis of a dimethoxyfulvene dialdehyde.

Reaction of dialdehyde **14** with dipyrrylmethane **15a** in presence to TFA gave the carbabenziporphyrin **12d** in 51% yield (Scheme 4). As expected, the presence of two methoxy-groups on this porphyrinoid system increased the aromatic characteristics compared to **12a-c**. The proton NMR spectrum for **12d** in $CDCl_3$ showed the *meso*-protons as four comparatively downfield singlets at 6.77, 7.26, 8.09 and 8.60 ppm (Figure 9). In addition, the internal CH protons for the indene and benzene units showed up at 3.84 and 4.88 ppm, respectively, relatively upfield values compared to the analogous protons in **12a**, which appeared at 4.97 and 6.03 ppm. Although the observed upfield and downfield shifts are still fairly weak for **12d**, they unambiguously attest to the presence of a global diamagnetic ring current (Figure 9).

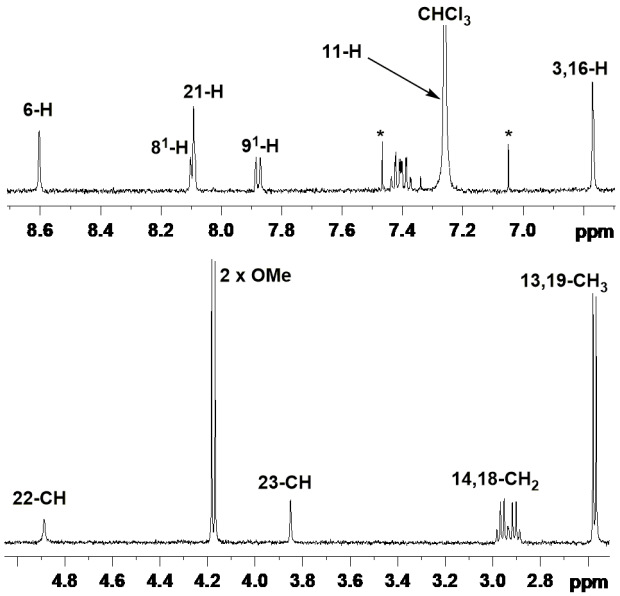

Figure 9. Partial proton NMR spectrum of dimethoxy-23-carbabenziporphyrin **12d** in $CDCl_3$ showing the internal 22-H and 23-H protons shifted to comparatively upfield values.

Addition of small amounts of TFA to solutions of **12d** gave the corresponding monocationic form **12d**H^+ (Scheme 5) and this species exhibited a further enhancement in macrocyclic aromaticity. The second methoxy group provides access to additional aromatic resonance

contributors such as **12d$^{R'}$**H^+ that also allow for further charge delocalization (Figure 5). As was the case for **12a**, the precise values for the observed proton resonances was dependent on the amount of TFA that was present. A typical proton NMR spectrum of **12d**H^+ in $CDCl_3$ with one drop of TFA showed the *meso*-protons at 6.85, 7.96, 8.45 and 8.83 ppm, while the internal protons on the indene and benzene units gave 1H singlets at 2.19 and 2.34 ppm ($\Delta\delta$ = 6.64 ppm). At much higher concentrations of TFA, the C-protonated dication **12d**H_2^{2+} was generated. Complete conversion of **12d** to the dicationic form was observed in 25% TFA-$CDCl_3$, while the monomethoxy-porphyrinoids **12a-c** were only completely converted into this form in 100% TFA. The proton NMR spectrum for dication **12d**H_2^{2+} showed that this species has a much stronger aromatic ring current and the difference in chemical shifts between the internal and external protons ($\Delta\delta$) was 11.43 ppm (Figure 10). The internal benzene proton gave a 1H singlet at 1.11 ppm, while the internal methylene resonance shifted further upfield to -0.71 ppm. Furthermore, the *meso*-protons were strongly deshielded giving rise to four 1H singlets at 9.58, 10.08, 10.57 and 10.72 ppm. The enhanced aromatic character can be attributed to the availability of further resonance contributors with 18π electron delocalization pathways such as **12d$^{R'}$**H_2^{2+} due to the presence of the second methoxy-substituent (Figure 5). When the proton NMR spectrum of **12d** was obtained in 100% *d*-TFA, the peaks corresponding to the internal NH and indene protons, and the resonance for the *meso*-proton at position 16, completely disappeared. This result again demonstrates that deuterium exchange readily occurs at these sites and in particular indicates that *meso*-protonated species such as **12d'**H_2^{2+} are in equilibrium with **12d**H_2^{2+} (Scheme 5).

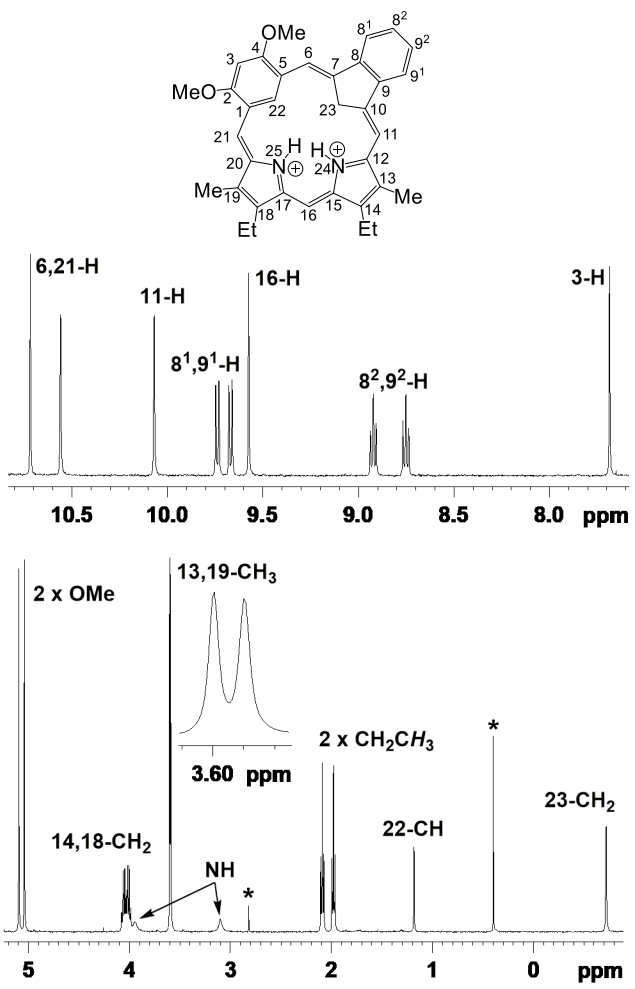

Figure 10. Partial proton NMR spectrum of dimethoxy-23-carbabenziporphyrin in 50% TFA-$CDCl_3$.

Fulvene dialdehyde **14** was also reacted with dipyrrylmethanes **15b** and **15c** to give dimethoxycarbabenziporphyrins **12e** and **12f** in 60% and 52% yields, respectively. The free base forms of **12d** and **12e** were insufficiently soluble to allow the carbon-13 NMR spectra to be obtained. However, **12f** had superior solubility characteristics and the carbon-13 NMR spectrum showed the *meso*-carbons at 95.0 (3-CH), 97.4 (11-CH), 112.7 (21-CH) and 116.1 ppm (6-CH), while the internal indene and benzene carbons appeared at 120.6 and 120.0 ppm, respectively. The UV-vis spectrum of free base **12e** in chloroform produced two broad peaks at 345 and 432

nm. Addition of TFA led to the formation of the related monocation **12e**H^+ and this gave broad peaks at 348 and 435 nm, followed by smaller bands between 500 and 800 nm. Titration of a solution of **12e** with TFA showed the gradual formation of **12e**H^+ with clear isosbestic points at 384 and 450 nm (Figure 12). The formation of the monocation was essentially complete upon addition of 10 equivalents of TFA. At higher concentrations of TFA, a dicationic species **12e**H_2^{2+} was generated and this showed a strong Soret-type band at 413 nm, followed by several Q-type bands (Figure 11).

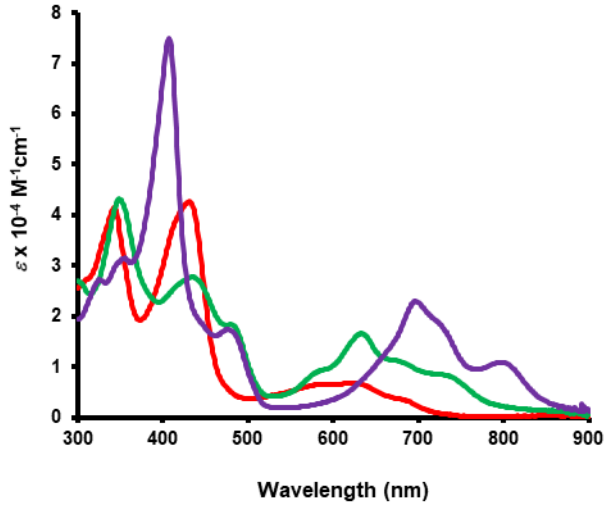

Figure 11. UV-vis spectra of **12e** in 1% triethylamine-dichloromethane (free base, red line), 1% TFA-dichloromethane (monocation **12e**H^+, green line) and TFA (dication **12e**H_2^{2+}, purple line).

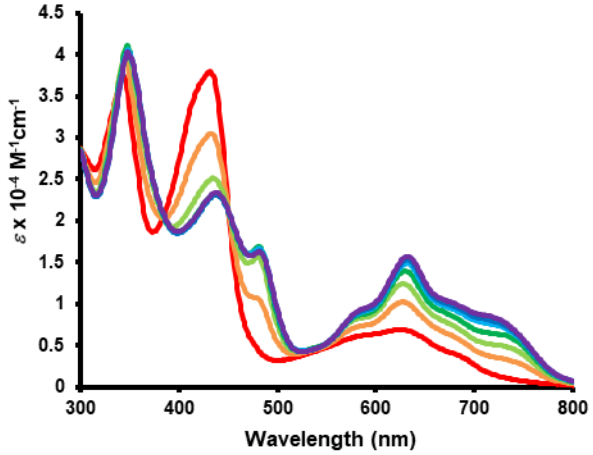

Figure 12. UV-vis spectra of **12e** in dichloromethane with incremental quantities of TFA: 0 equiv (red line), 0.5 equiv (orange) 1 equiv (light green), 2 equiv (dark green), 5 equiv (light blue), 10 equiv (dark blue) and 20 equiv (purple).

The electron impact mass spectra for **12a-f** showed strong $[M + 2H]^+$ peaks and in some cases high resolution data could not be obtained for the molecular ions. This phenomenon has previously been observed for benziporphyrins **6**.[11] However, TOF ESI MS gave the expected $[M + H]^+$ peaks in each case and the high resolution data confirmed the expected molecular formulae for these structures.

Computational Investigations

Further insights into the relative stabilities and aromatic characteristics of tautomeric benzo-23-carbabenziporphyrins (BCBs) and related protonated species were obtained by performing DFT calculations. Initially, the unsubstituted BCB system was investigated (Table 1), and the structures were optimized using B3LYP with the triple-ζ basis set 6-311+ +G(d,p).[41] Eight tautomeric forms were considered where one hydrogen is relocated to one of eight positions, and these structures have been designated to show the positions of those hydrogens, e.g. as **BCB-24H**, **BCB-23H**, etc. The relative stabilities of the tautomers were assessed using three different

functionals, B3LYP, M06-2X, and B3LYP-D3,[42,43] and the relative Gibbs free energy was also determined with B3LYP. The results obtained using each of these methods were very similar. In addition, the relative ΔG values showed the same trends as the relative ΔE values, indicating that entropic factors were not significant. The lowest energy tautomers were **BCB-24H** and **BCB-25H** and these differed in energy by only slightly over 1 kcal/mol (Table 1).

Table 1. Calculated Relative Energies (kcal/mol) and NICS Values (ppm) for Selected Unsubstituted Benzo-23-carbabenziporphyrin Tautomers. Bold: strongly shielded (aromatic); red: strongly deshielded.

	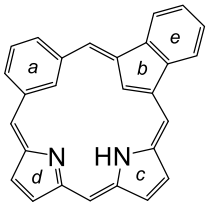	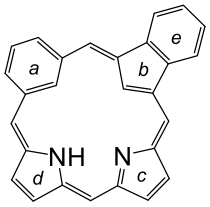	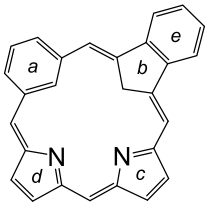	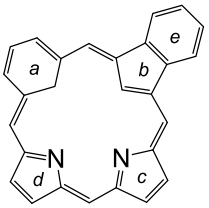
Molecule	**BCB-24H**	**BCB-25H**	**BCB-23H**	**BCB-22H**
ΔG (298 K)	0.00	+0.96	+14.59	+26.07
ΔE (B3LYP/ **M06-2X**/ B3LYP-D3)	(0.00/ **0.00**/ 0.00)	(+1.21/ **+1.36**/ +1.26)	(+15.75/ **+14.05**/ +15.94)	(+27.72/ **+33.17**/ +27.85)
NICS(0)/NICS(1)$_{zz}$	-0.12/+1.43	-0.27/+0.56	+0.49/ +4.46	**-12.70/-30.96**
NICS(a)/NICS(1a)$_{zz}$	**-6.53/-21.34**	**-7.45/-21.78**	**-6.42/-21.88**	**-16.09/-47.37**
NICS(b)/NICS(1b)$_{zz}$	+2.95/+5.24	+3.56/+3.74	+1.51/ -1.01	**+11.44/+23.52**
NICS(c)/NICS(1c)$_{zz}$	-4.09/-9.86	-0.68/-7.46	+0.99/ -4.74	+0.54/-7.07
NICS(d)/NICS(1d)$_{zz}$	-0.77/-7.85	-3.70/-8.09	-1.07/ -8.56	+0.73/-6.76
NICS(e)/NICS(1e)$_{zz}$	**-6.96/-23.69**	**-6.81/-22.45**	**-6.79/-23.61**	**-3.94/-15.96**

Table 2. Dihedral angles between individual subunits in selected benzo-23-carbabenziporphyrins and related protonated species.

Molecule	*ab*	*bc*	*cd*	*da*	Average
BCB-24H	-17.73	-10.93	1.43	-10.16	**10.06**
BCB-25H	-18.15	7.83	-1.31	13.34	**10.16**
BCB-24,25H$^+$	27.04	-19.92	14.02	-22.00	**20.75**
BCB-23,24,25H^{2+}	10.83	-6.36	-15.36	-18.97	**12.88**
MeOBCB-24H	-15.54	10.22	-1.73	-9.30	**9.20**
MeOBCB-25H	-15.90	6.85	-1.54	12.88	**9.29**
MeOBCB-24,25-H$^+$	24.54	-18.92	14.33	-21.90	**19.92**
MeOBCB-23,24,25-H^{2+}	8.48	-6.53	15.34	-18.02	**12.09**
MeO$_2$BCB-24H	-17.28	11.00	-1.90	9.54	**9.93**
MeO$_2$BCB-25H	-17.44	8.11	-1.55	12.27	**9.84**
MeO$_2$BCB-24,25H$^+$	25.53	-19.50	14.01	-20.72	**19.94**
MeO$_2$BCB-23,24,25H^{2+}	7.91	-7.08	15.12	-16.41	**11.63**

The individual rings within these macrocycles are twisted relative to one another by about 10^o (Table 2) due to crowding within the porphyrinoid cavity. The favored **BCB** tautomers have three hydrogens within the macrocycle and are cross-conjugated due to the presence of the arene ring. **BCB-23H**, which possesses an internal methylene unit, is ca. 15 kcal/mol higher in energy, while the aromatic tautomer **BCB-22H**, which sacrifices the 6π electron character of the benzene unit, is between 26.07 and 33.17 kcal/mol higher in energy. In fact, tautomers with interrupted conjugation due to the presence of CH_2 bridges are lower in energy than **BCB-22H** despite the presence of an 18π electron delocalization pathway in the latter structure (Table S1). Nucleus-independent chemical shift (NICS) calculations were performed,[44] and these confirmed that only tautomer **BCB-22H** possesses global diatropic character. Large negative NICS values indicate that a structure is aromatic, while antiaromatic compounds give large positive values and nonaromatic species afford results that are close to zero. Standard NICS calculations are considered to be less accurate as the effects due to σ and π electrons are included and these results may not always reliably assess aromatic properties. For this reason, $NICS_{ZZ}$ calculations

were also conducted because these primarily assess the effects caused by the π system. These calculations were performed 1 Å above the ring ($NICS(1)_{ZZ}$) and give numerical values that are substantially larger than those given by NICS. As the same trends were observed using both methods, the discussion focuses on the standard NICS results in order to avoid confusion. The *m*-phenylene (ring *a*) and benzo-units (ring *e*) NICS values for the nonaromatic tautomers both gave significantly negative values in the range of -6.17 to -7.58 ppm, demonstrating that these units retained strong localized aromatic characteristics. The aromatic ring currents within a macrocycle due to an applied magnetic field can also be assessed by anisotropy of induced current density (AICD)[45] and these calculations were performed on all of the tautomers. Figure 13 shows the AICD plots for the low energy tautomer **BCB-24H** and the high energy aromatic form **BCB-22H**. No global delocalization pathway is evident for **BCB-24H**, but a clear 18π electron delocalization pathway is evident for **BCB-22H**.

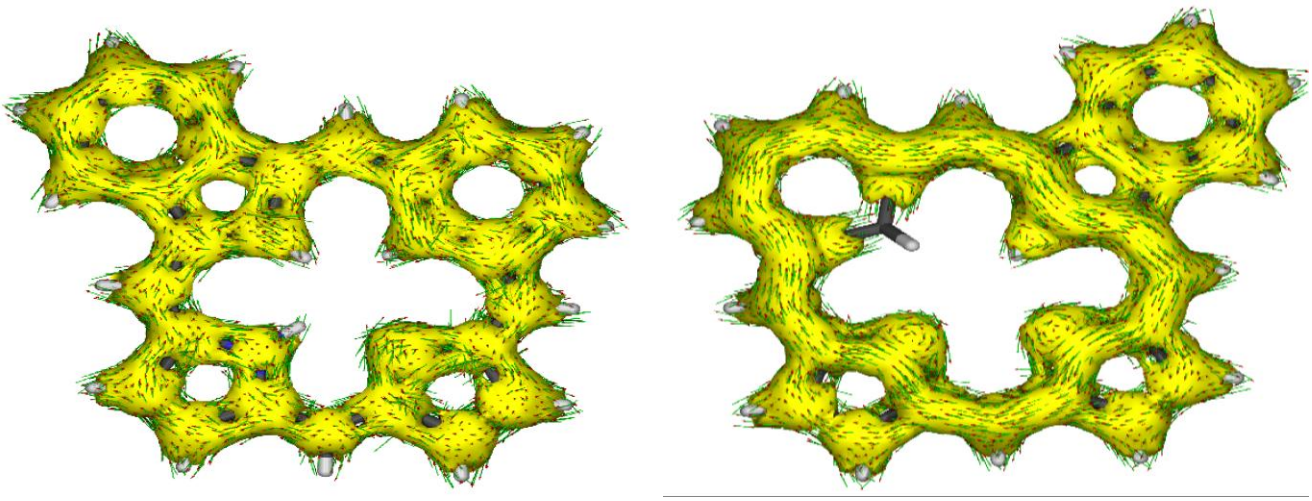

Figure 13. AICD plots for **BCB-24H** and **BCB-22H**. The latter shows a clear 18π electron delocalization pathway.

Five monoprotonated species were considered (Table 3). Although the expected tautomer **BCB-24,25H**$^+$ was favored, tautomers **BCB-23,24H**$^+$ and **BCB-23,25H**$^+$ with internal CH_2's on

the indene unit were only 1.06-3.53 kcal/mol higher in energy. The increased crowding within the cavity leads to further distortions to the macrocycle (Table 2). Protonation onto the internal benzene carbon is not favorable as tautomers **BCB-22,25H**$^+$ and **BCB-22,24H**$^+$ are 12.24-20.48 kcal/mol higher in energy. However, NICS calculations indicate that these high energy tautomers are the only ones that possess significant global aromatic character. The instability of the arene-protonated structures can be attributed to the magnitude of the macrocyclic aromaticity being insufficient to offset the loss of the thermodynamically favored benzene subunit. The formation of dications requires C-protonation and the expected indene-protonated form **BCB-23,24,25H**$^{2+}$ was shown to be 11.70-16.14 kcal.mol lower in energy than the benzene protonated form **BCB-23,24,25H**$^{2+}$ (Table 4). NICS calculations show that **BCB-23,24,25H**$^{2+}$ exhibits weakly aromatic properties (NICS(0) = -3.01 ppm) but the high energy tautomer exhibits a much larger diamagnetic ring current (NICS(0) = -13.33 ppm).

Table 3. Calculated Relative Energies (kcal/mol) and NICS Values (ppm) for Tautomers of Monoprotonated Benzo-23-carbabenziporphyrin. Bold: strongly shielded (aromatic); red: strongly deshielded.

	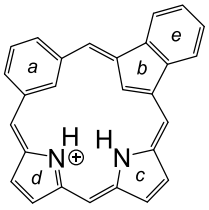	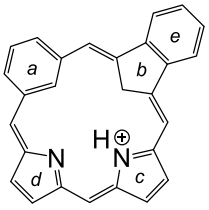	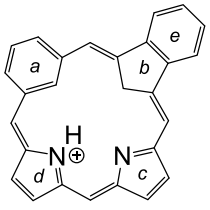	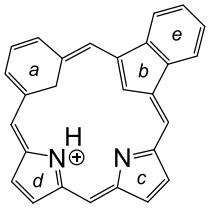	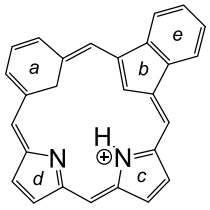
Molecule	**BCB-24,25H**$^+$	**BCB-23,24H**$^+$	**BCB-23,25H**$^+$	**BCB-22,25H**$^+$	**BCB-22,24H**$^+$
ΔG (298 K)	0.00	+1.06	+1.89	+13.21	+12.24
ΔE (B3LYP/ **M06-2X**/ B3LYP-D3)	(0.00/ **0.00**/ 0.00)	(+1.43/ **+2.50**/ +1.91)	(+2.51/ **+3.53**/ +2.87)	(+14.33/ **+20.48**/ +14.83)	(+13.26/ **+19.36**/ +13.77)
NICS(0)/NICS(1)$_{zz}$	-1.03/-0.03	-1.33/-0.16	-1.44/-0.67	**-13.32/-32.49**	**-13.49/-32.66**
NICS(a)/NICS(1a)$_{zz}$	**-5.97/-16.55**	**-4.80/-17.79**	**-5.72/-18.77**	**-16.78/-49.13**	**-16.73/-48.87**
NICS(b)/NICS(1b)$_{zz}$	+3.43/+5.63	-0.64/-5.94	-0.40/-5.92	**+15.43/+33.71**	**+13.62/+32.45**
NICS(c)/NICS(1c)$_{zz}$	-5.76/-12.27	-4.87/-13.09	+3.71/+1.60	+0.13/-7.91	**-11.25/-31.40**
NICS(d)/NICS(1d)$_{zz}$	**-4.94/-16.80**	-2.62/-11.69	**-5.74/-15.23**	**-11.26/-30.06**	+0.35/-6.33
NICS(e)/NICS(1e)$_{zz}$	**-7.00/-23.54**	**-6.70/-23.73**	**-6.89/-24.46**	-2.62/-12.35	-3.23/-13.19

Table 4. Calculated Relative Energies (kcal/mol) and NICS Values (ppm) for Benzo-23-carbabenziporphyrin Dications. Bold: strongly shielded (aromatic); red: strongly deshielded.

	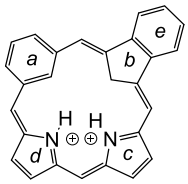	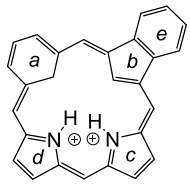
Molecule	**BCB-23,24,25H^{2+}**	**BCB-22,24,25H^{2+}**
ΔG (298 K)	0.00	+11.70
ΔE (B3LYP/ **M06-2X**/ B3LYP-D3)	(0.00/ **0.00**/ 0.00)	(+12.28/ **+16.14**/ +12.36)
NICS(0)/NICS(1)$_{zz}$	-3.01/-4.25	**-13.33/-29.99**
NICS(a)/NICS(1a)$_{zz}$	-3.60/-11.91	**-15.70/-46.95**
NICS(b)/NICS(1b)$_{zz}$	-3.04/-12.17	**+18.33/+47.59**
NICS(c)/NICS(1c)$_{zz}$	-4.63/-9.21	**-19.20/-48.20**
NICS(d)/NICS(1d)$_{zz}$	**-7.80/-23.78**	**-12.21/-22.90**
NICS(e)/NICS(1e)$_{zz}$	**-6.53/-24.69**	-0.38/-5.48

2-Methoxybenzocarbabenziporphyrins (**MeOBMB**s) were also investigated and for the most part the free base tautomers showed similar trends (Table 5). Again the 24H tautomer was slightly more stable than the 25H form, while the fully aromatic tautomer **MeOBCB-22H** was approx. 30 kcal/mol higher in energy. However, the NICS calculations suggest that **MeOBCB-24H** and **MeOBCB-25H** possess weak diatropic character, although the NICS(0) values were only -1.35 and -1.42 ppm, respectively. Monoprotonation was still favored on the nitrogens to give **MeOBCB-24,25H^{+}**, but protonation onto the inner indene carbon gave tautomers that were only 1.27-3.10 kcal/mol higher in energy (Table 6). All three of these tautomers have higher negative NICS values ranging from -3.00 to -3.30 ppm, and these results are in general agreement with experimental observations. Nevertheless, the AICD plot for **MeOBCB-24,25H^{+}** does not show clear global delocalization pathways (Figure 14). Protonation onto the *m*-phenylene unit can give tautomers **MeOBCB-22,25H^{+}** and **MeOBCB-22,24H^{+}**, both of which have strong diamagnetic ring currents, but these are 12.78-19.46 kcal/mol higher in energy. The

most stable monoprotonated form, which is consistent with the observed monocations derived from **12a-c**, gives a positive NICS value for ring *b* and negative values for rings *c* and *d*, and these results suggest that resonance contributors such as **12^{R}**H^{+} are responsible for the increased diatropic character. Diprotonation onto the interior of the macrocycle might give rise to C-protonation onto the indene or benzene units. However, the latter species, **MeOBCB-22,24,25H^{2+}**, is much higher in energy (Table 7). The indene-protonated structure **MeOBCB-23,24,25H^{2+}** shows a significant increase in diatropic character (NICS(0) = -5.81 ppm) and rings *b*, *c* and *d* all gave large negative NICS values. This indicates that the macrocyclic ring current goes around the outside of these rings and indicates that conjugation pathways such as the 22π electron system found in **31** (Figure 15) are responsible for the diatropic ring currents observed for **12a-c**H_2^{2+}. The AICD plot for **MeOBCB-23,24,25H^{2+}** confirms the presence of global delocalization pathways and also suggests that the 22π electron circuit is favored (Figure 14).

Table 5. Calculated Relative Energies (kcal/mol) and NICS Values (ppm) for 2-Methoxy-benzo-23-carbabenziporphyrin Tautomers. Bold: strongly shielded (aromatic); red: strongly deshielded.

	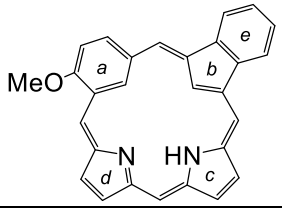	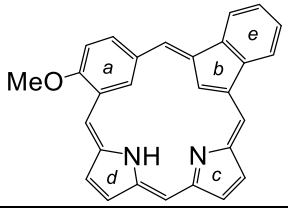	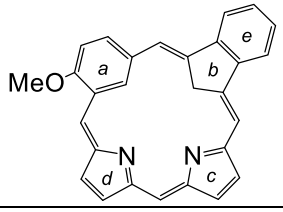	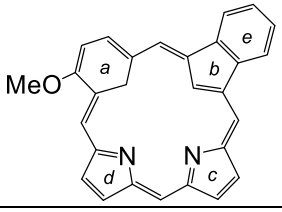
Molecule	**MeOBCB-24H**	**MeOBCB-25H**	**MeOBCB-23H**	**MeOBCB-22H**
ΔG (298 K)	0.00	+0.98	+14.93	+26.44
ΔE (B3LYP/ **M06-2X**/ B3LYP-D3)	(0.00/ **0.00**/ 0.00)	(+1.23/ **+1.36**/ +1.28)	(+16.19/ **+14.26**/ +16.37)	(+28.16/ **+32.55**/ +28.29)
NICS(0)/NICS(1)$_{zz}$	-1.35/-1.67	-1.42/-2.16	0.23/+2.84	**-11.52/-27.54**
NICS(a)/NICS(1a)$_{zz}$	**-5.67/-15.23**	**-6.90/-17.35**	**6.08/-17.52**	**-15.13/-41.34**
NICS(b)/NICS(1b)$_{zz}$	+2.95/+3.34	+3.61/+4.22	+0.79/-2.84	**+9.27/+18.24**
NICS(c)/NICS(1c)$_{zz}$	-4.89/-12.64	-0.95/-8.38	+0.81/-5.16	-0.50/-9.01
NICS(d)/NICS(1d)$_{zz}$	-1.14/-8.13	-4.41/-9.75	-1.37/-9.27	-0.22/-8.66
NICS(e)/NICS(1e)$_{zz}$	**6.84/-22.39**	**-6.78/-22.35**	**-7.04/-24.00**	**-4.74/-17.67**

Table 6. Calculated Relative Energies (kcal/mol) and NICS Values (ppm) for Tautomers of 2-Methoxy-benzo-23-carbabenziporphyrin Monocations. Bold: strongly shielded (aromatic); red: strongly deshielded.

	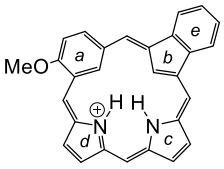	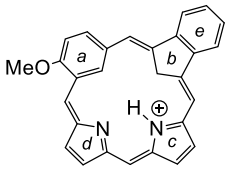	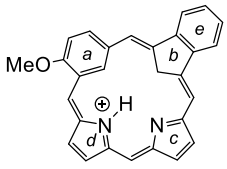	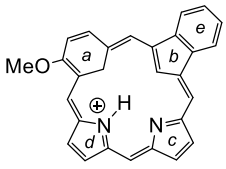	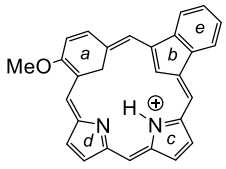
Molecule	**MeOBCB-24,25H$^+$**	**MeOBCB-23,24H$^+$**	**MeOBCB-23,25H$^+$**	**MeOBCB-22,25H$^+$**	**MeOBCB-22,24H$^+$**
ΔG (298 K)	0.00	+1.27	+1.78	+13.69	+12.78
ΔE (B3LYP/ **M06-2X**/ B3LYP-D3)	(0.00/ **0.00**/ 0.00)	(+1.67/ **+2.54**/ +2.13)	(+2.74/ **+3.45**/ +3.10)	(+14.88/ **+19.46**/ +15.37	(+13.93/ **+18.61**/ +14.43)
NICS(0)/NICS(1)$_{zz}$	-3.30/-5.86	-3.00/-4.43	-3.00/-5.10	**-11.35/-27.19**	**-11.81/-28.12**
NICS(a)/NICS(1a)$_{zz}$	-4.51/-8.86	-2.89/-10.01	-3.84/-12.24	**-14.69/-40.63**	**-14.86/-41.24**
NICS(b)/NICS(1b)$_{zz}$	+3.75/+5.81	-2.63/-11.11	-2.25/-11.25	**+12.63/+26.77**	**+10.86/+25.16**
NICS(c)/NICS(1c)$_{zz}$	-7.14/-13.85	**-5.98/-15.84**	+3.04/-0.47	-0.74/-9.36	**-11.73/-31.61**
NICS(d)/NICS(1d)$_{zz}$	**-6.45/-22.10**	-3.17/-13.16	**-7.01/-17.74**	**-12.12/-31.53**	-1.09/-9.55
NICS(e)/NICS(1e)$_{zz}$	**-6.87/-23.14**	**-7.48/-25.33**	**-7.52/-25.62**	**-3.81/-15.13**	**-4.32/-15.72**

Table 7. Calculated Relative Energies (kcal/mol) and NICS Values (ppm) for Unsubstituted 2-Methoxy-benzo-23-carbabenziporphyrin Dications. Bold: strongly shielded (aromatic); red: strongly deshielded.

	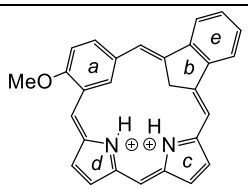	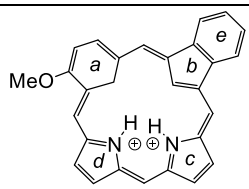
Molecule	**MeOBCB-23,24,25H^{2+}**	**MeOBCB-22,24,25H^{2+}**
ΔG (298 K)	0.00	+12.50
ΔE (B3LYP/ **M06-2X**/ B3LYP-D3)	(0.00/ **0.00**/ 0.00)	(+13.00/ **+14.85**/ +13.05)
NICS(0)/NICS(1)$_{zz}$	-5.81/-11.97	**-10.14/-22.84**
NICS(a)/NICS(1a)$_{zz}$	-0.22/-4.28	**-12.03/-35.12**
NICS(b)/NICS(1b)$_{zz}$	**-6.23/-21.88**	**+15.08/+37.64**
NICS(c)/NICS(1c)$_{zz}$	**-6.68/-24.01**	**-11.11/-36.23**
NICS(d)/NICS(1d)$_{zz}$	**-9.99/-20.52**	**-12.93/-24.60**
NICS(e)/NICS(1e)$_{zz}$	**-7.97/-27.25**	-1.97/-9.48

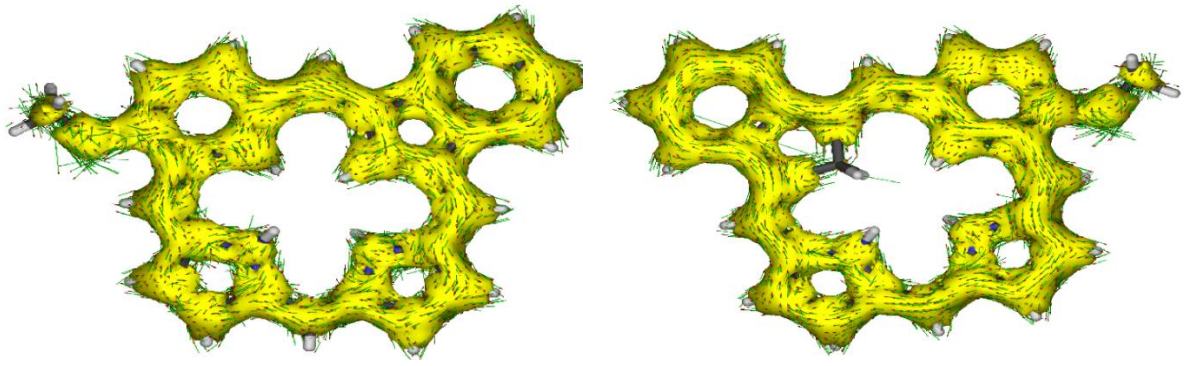

Figure 14. AICD plots of **MeOBCB-24,25H**$^{+}$ and **MeOBCB-23,24,25-H**$^{2+}$.

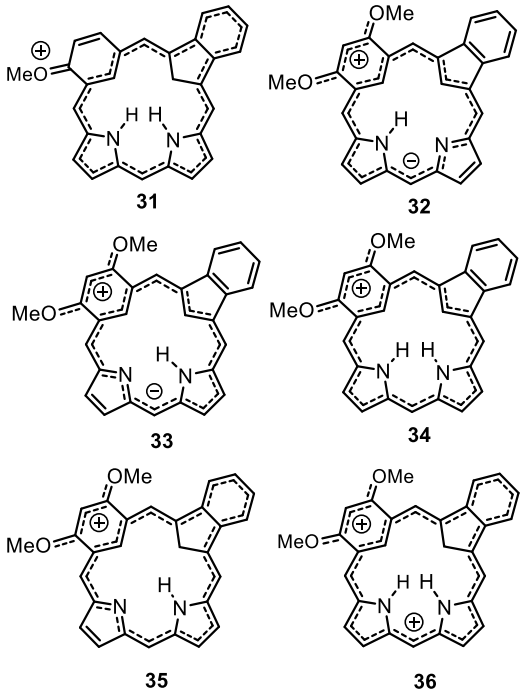

Figure 15. Potential delocalization pathways in methoxy- and dimethoxy-23-carbabenziporphyrins and related protonated species.

Table 8. Calculated Relative Energies (kcal/mol) and NICS Values (ppm) for 2,4-Dimethoxy-benzo-23-carbabenziporphyrin Tautomers. Bold: strongly shielded (aromatic); red: strongly deshielded.

	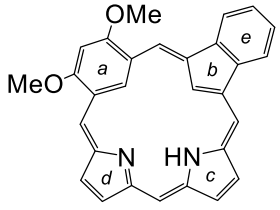	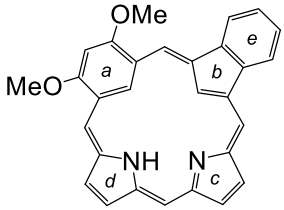	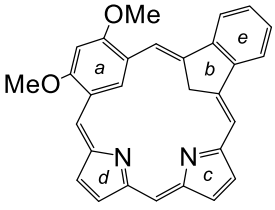	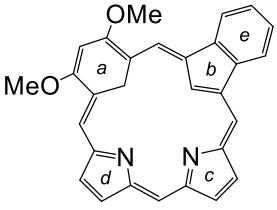
Molecule	**MeO_2BCB-24H**	**MeO_2BCB-25H**	**MeO_2BCB-23H**	**MeO_2BCB-22H**
ΔG (298 K)	0.00	+1.38	+15.02	+27.07
ΔE (B3LYP/ **M06-2X**/ B3LYP-D3)	(0.00/ **0.00**/ 0.00)	(+1.68/ **+1.93**/ +1.75)	(+16.33/ **+14.50**/ +16.52)	(+28.97/ **+32.61**/ +29.10)
NICS(0)/NICS(1)$_{zz}$	-2.41/-4.32	-2.57/-5.03	-0.71/+1.53	**-10.22/-23.90**
NICS(a)/NICS(1a)$_{zz}$	-4.81/-10.23	-6.05/-12.56	-5.59/-13.19	**-14.38/-35.93**
NICS(b)/NICS(1b)$_{zz}$	+2.92/+3.70	+3.66/+4.72	+0.32/-4.49	**+8.36/+15.86**
NICS(c)/NICS(1c)$_{zz}$	**-5.40/-14.35**	-1.07/-9.17	+0.48/-5.83	**-1.10/-15.86**
NICS(d)/NICS(1d)$_{zz}$	-1.83/-9.60	-5.25/-11.46	-2.05/-10.86	-1.87/-12.02
NICS(e)/NICS(1e)$_{zz}$	**-6.70/-21.60**	**-6.58/-21.77**	**-7.17/-24.30**	**-4.89/-18.31**

Dimethoxy-BCBs (**MeO_2BCB**s) exhibit further increases in aromatic character, although the macrocycles still show a significant degree of distortion (Table 2). Once again, the tautomer with a proton of N24 was favored, although the closely related form **MeO_2BCB-25H** was less than 2 kcal/mol higher in energy (Table 8). For the 8 free base tautomers considered, the fully aromatic form **MeO_2BCB-22H** was the highest in energy, followed by the four versions with CH_2 bridges (Tables 8 and S3). Tautomer **MeO_2BCB-23H** with an internal CH_2 on the indene unit has no overall aromatic character and is ca. 15 kcal/mol higher in energy than the most stable form. The two lowest energy tautomers, **MeO_2BCB-24H** and **MeO_2BCB-25H**, gave NICS(0) values of ca. -2.5 ppm and these indicate the presence of a strengthened, albeit small, diatropic ring current. This is compatible with the proton NMR spectra obtained for **12d-f**. For **MeO_2BCB-24H**, the emergence of this property is consistent with contributions from dipolar species such as **32**

(Figure 15) and it is notable that ring *c* shows a larger negative NICS value than rings *b* or *d* (the latter gives a small positive value). Similarly, **MeO$_2$BCB-25H** gives a greater negative value for ring *d* than ring *c*, and ring *b* gave a positive result, and these data indicate that dipolar species such as **33** may be responsible for the weak macrocyclic diatropicity. It should be noted that species of this type are proposed to contribute to the aromatic properties but the major canonical form is still likely to be the original cross-conjugated structure. Five monoprotonated tautomers were considered, all of which show medium to strong diatropic ring currents (Table 9). The benzene-protonated structures are much higher in energy than the other three. The lowest energy form, **MeO$_2$BCB-24,25H$^+$**, gives a NICS(0) value of -5.18 ppm and shows strongly negative NICS values for rings *c* and *d*. This implies that delocalized contributors such as **34** with 18π electron pathways are favored (Figure 15). These calculated results are in good agreement with the proton NMR spectra obtained for **12d-f**H$^+$. The AICD plot for **MeO$_2$BCB-24,25H$^+$** also shows the presence of macrocyclic delocalization pathways (Figure 16). The indene-protonated cations **MeO$_2$BCB-23,24H$^+$** and **MeO$_2$BCB-23,25H$^+$** are only slightly higher in energy and show slightly reduced diatropicity. Nevertheless, similar delocalization pathways, e.g. **35**, can be used to explain the emergence of aromaticity in these structures. The relatively large negative NICS value for the benzo-unit (ring e) also suggests that 22π electron delocalization pathways may be involved. The favored dicationic species **MeO$_2$BCB-23,24,25H^{2+}** is C-protonated onto the interior indene carbon and this structure shows an additional increase to the ring current (NICS(0) = -6.93 ppm) compared to the favored monocation (Table 10). The large negative NICS values for rings *b*, *c*, *d* and *e* are consistent with significant contibutions from a 23-atom 22π electron delocalized structures such as **36**. This conjugation pathway is clearly evident in the AICD plot for this species (Figure 16).

Table 9. Calculated Relative Energies (kcal/mol) and NICS Values (ppm) for Monoprotonated 2,4-Dimethoxy-benzo-23-carbabenziporphyrin Tautomers. Bold: strongly shielded (aromatic); red: strongly deshielded.

	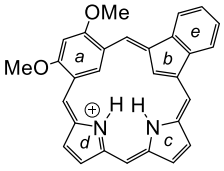	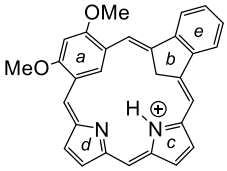	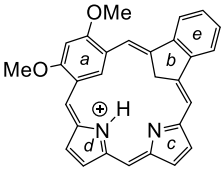	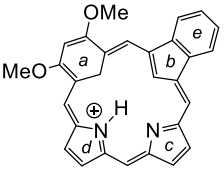	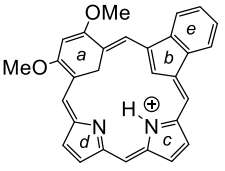
Molecule	**MeO_2BCB-24,25H$^+$**	**MeO_2BCB-23,24H$^+$**	**MeO_2BCB-23,25H$^+$**	**MeO_2BCB-22,25H$^+$**	**MeO_2BCB-22,24H$^+$**
ΔG (298 K)	0.00	+0.91	+1.06	+14.29	+13.45
ΔE (B3LYP/ **M06-2X**/ B3LYP-D3)	(0.00/ **0.00**/ 0.00)	(+1.23/ **+2.04**/ +1.70)	(0.00/ **0.00**/ 0.00)	(+15.59/ **+18.38**/ +16.07)	(+14.49/ **+17.58**/ +14.99)
NICS(0)/NICS(1)$_{zz}$	-5.18/-10.37	-4.11/-7.38	-3.84/-7.24	**-8.50/-19.45**	**-9.26/-21.20**
NICS(a)/NICS(1a)$_{zz}$	-2.83/-5.39	-1.28/-3.37	-2.24/-5.25	**-11.64/-29.79**	**-12.19/-31.27**
NICS(b)/NICS(1b)$_{zz}$	+4.13/+8.06	**-3.89/-14.72**	**-3.31/-14.03**	**+10.37/+21.27**	**+8.80/+20.03**
NICS(c)/NICS(1c)$_{zz}$	**-8.15/-26.41**	**-7.12/-18.51**	+2.21/-2.01	-0.91/-9.29	**-11.35/-30.11**
NICS(d)/NICS(1d)$_{zz}$	**-8.08/-14.32**	**-4.00/-15.20**	**-8.36/-21.24**	**-12.09/-30.53**	-2.59/-12.33
NICS(e)/NICS(1e)$_{zz}$	**-6.61/-20.06**	**-7.92/-26.56**	**-7.97/-26.82**	**-4.44/-17.10**	**-4.90/-17.36**

Table 10. Calculated Relative Energies (kcal/mol) and NICS Values (ppm) for 2,4-Dimethoxy-benzo-23-carbabenziporphyrin Dications. Bold: strongly shielded (aromatic); red: strongly deshielded.

	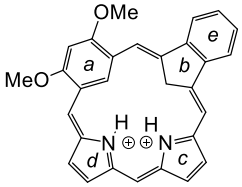	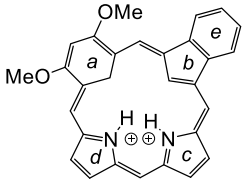
Molecule	**MeO_2BCB-23,24,25H^{2+}**	**MeO_2BCB-22,24,25H^{2+}**
ΔG (298 K)	0.00	+13.60
ΔE (B3LYP/ **M06-2X**/ B3LYP-D3)	(0.00/ **0.00**/ 0.00)	(+14.16/ **+14.19**/ +14.15)
NICS(0)/NICS(1)$_{zz}$	**-6.93/-14.91**	**-6.78/-14.08**
NICS(a)/NICS(1a)$_{zz}$	+1.96/+3.26	**-8.29/-22.49**
NICS(b)/NICS(1b)$_{zz}$	**-7.43/-24.85**	**+12.16/+29.00**
NICS(c)/NICS(1c)$_{zz}$	**-8.00/-27.64**	**-9.54/-30.52**
NICS(d)/NICS(1d)$_{zz}$	**-11.60/-23.65**	**-12.30/-23.69**
NICS(e)/NICS(1e)$_{zz}$	**-8.78/-28.87**	-3.22/-12.37

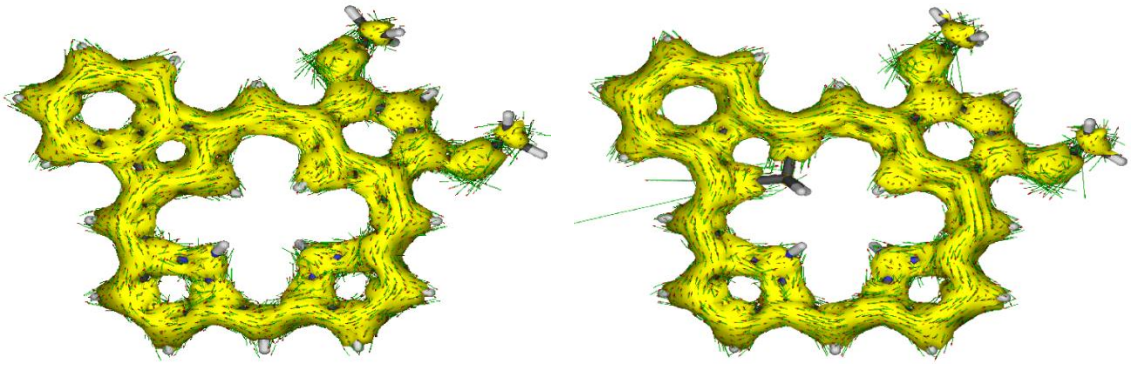

Figure 16. AICD plots of **MeO$_2$BCB-24,25-H$^+$** and **MeO$_2$BCB-23,24,25H^{2+}**.

Selective Oxidation of 23-Carbabenziporphyrins with Silver(I) Acetate

Carbabenziporphyrins **12a-f** are stable porphyrinoids and show little decomposition after several weeks in solution. In this respect, the *adj*-dicarbaporphyrins differ considerably from *opp*-dicarbaporphyrins that have been shown to have poor stability characteristics.[1] Therefore, these *adj*-dicarbaporphyrins show promise for further investigations. Attempts to prepare silver(III) derivatives **37** of these porphyrinoids were not successful but selective oxidation reactions were observed instead (Scheme 7). Dicarbaporphyrinoids **12a**, **12d** and **12f** were stirred with silver(I) acetate at room temperature in dichloromethane-methanol. Following work up, the products were purified by column chromatography on grade 3 neutral alumina and a deep purple fraction was collected. The UV-vis spectra for the products from all three reactions were essentially identical, indicating that the chromophores were not affected by the presence of a second methoxy-substituent on the arene unit. Specifically, the UV-vis spectrum for the product derived from **12a** gave two strong broad bands at 342 and 578 nm (Figure 17). Significantly, the proton NMR spectra for the oxidation products showed the presence of two additional methoxy groups. The proton NMR spectrum of the major product derived from **12a** gave a 3H singlet for the 3-methoxy substituent at 3.77 ppm together with two additional 3H singlets at 3.39 and 3.42 ppm (Figure 18). The *meso*-protons gave rise to resonances at 5.68, 5.90, 6.67 and 7.12 ppm,

three of which showed weak long-range coupling interactions. Not only do these values demonstrate that the macrocycle possesses no global aromatic character, but the HSQC spectrum also showed that the two upfield *meso*-protons correlated with carbon-13 resonances at 71.1 and 71.8 ppm, confirming that these bridges are sp^3 hybridized. Furthermore, the chemical shifts and nOe difference NMR data demonstrated that methoxy-substituents had been introduced at the 6- and 21-positions. The internal NH was observed as a broad peak at 11.22 ppm, while the internal indene and arene protons appeared at 6.99 and 8.09 ppm, respectively. These data showed that the product of this reaction was the trimethoxy-dihydrocarbabenziporphyrin **38a**. Reaction of **12d** and **12f** with silver(I) acetate similarly afforded the closely related nonaromatic porphyrinoids **38b** and **38c**, respectively. As the benzene subunit is disconnected from the conjugated fragment for these molecules, the chromophores would not be expected to be altered by the presence of additional methoxy groups. The NMR data for these derivatives clearly showed that a single isomer had been isolated. In principle, these reactions could produce *cis*- or *trans*- isomers but the spectroscopic results could not distinguish between these two possibilities. As the NMR results clearly show that only one diastereomer is favored, the reactions are stereoselective, although these chiral products would be generated in racemic form. The yields for **38a-c** ranged from 32-45%.

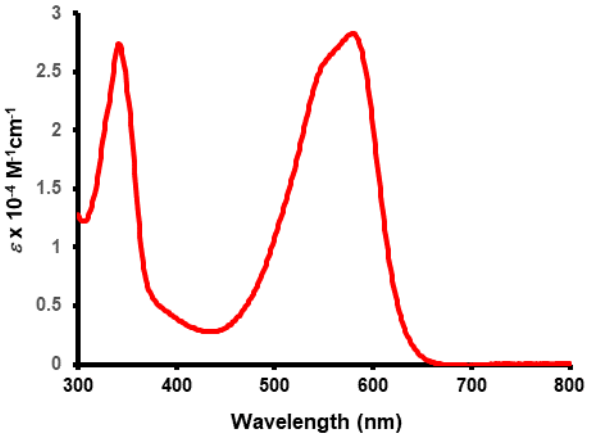

Figure 17. UV-vis spectrum of the oxidation product **38a** in dichloromethane.

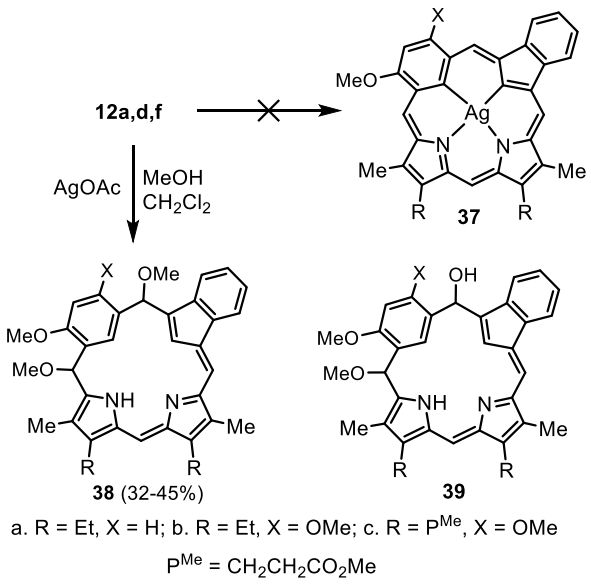

Scheme 7. Reaction of silver(I) acetate with 23-carbabenziporphyrins.

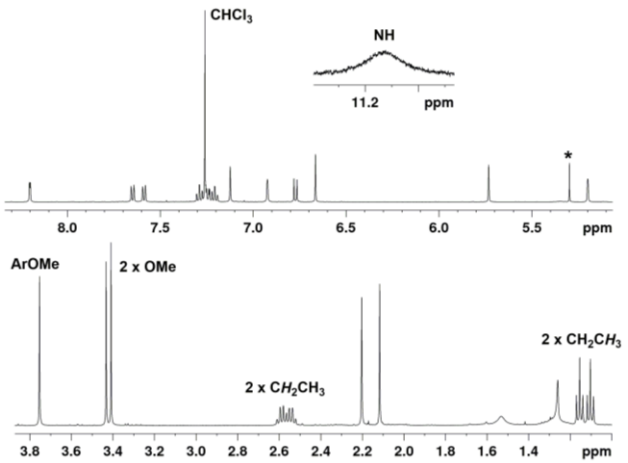

Figure 18. 500 MHz proton NMR spectrum of **38a** in $CDCl_3$.

Column chromatography gave a major purple fraction in these reactions, but a minor, more polar, purple band was also observed. The appearance of this band was remarkably similar to the major product, and the UV-vis spectra were also virtually identical to those obtained for **38a-c**. The minor products from the reactions of **12a** and **12d** with silver(I) acetate were isolated and spectroscopically identified. The proton NMR spectrum for the minor product derived from **12a** in $CDCl_3$ showed the presence of only two OMe groups at 3.43 and 3.75 ppm, indicating that only one molecule of methanol had been incorporated. Two of the bridging CH protons were identified as aliphatic units at 5.73 and 5.74 ppm in the proton NMR spectrum and 71.5 and 72.2 ppm in the carbon-13 NMR spectrum, strongly implying that these units are connected to oxygen atoms. High resolution TOF ESI MS gave the $[M + H]^+$ peak at *m/z* 533.2798. This corresponds to the molecular formula $C_{35}H_{37}N_2O_3$ and indicates that while only one methyl group has been introduced, two oxygen atoms have been incorporated. Although a peak corresponding to an OH could not be identified when the proton NMR spectra were obtained in $CDCl_3$ or d_6-benzene, the data were otherwise consistent with a product analogous to **38a** with a hydroxyl substituent in

place of one of the methoxy groups. This could plausibly arise by reaction with trace amounts of water. Nevertheless, a single regioisomer had been generated. When the proton NMR spectrum was run in d_6-DMSO, two doublets and a singlet were noted between 5.55 and 5.70 ppm (Figure 19). The ^{1}H-^{1}H COSY spectrum demonstrated that the doublets coupled to one another. However, while the HSQC spectrum showed that the singlet at 5.68 ppm and the doublet at 5.57 ppm correlated with carbon-13 resonances at 68.5 and 70.8 ppm, the doublet at 5.67 ppm showed no connection and therefore can be assigned as the hydroxyl proton (Figure 19). The sp^2 methine protons showed up at 6.67 and 7.15 ppm in $CDCl_3$, while the corresponding carbon resonances appeared at 116.1 and 116.5 ppm. The identity of the isolated regioisomer was determined to be **39a** using homonuclear nOe difference proton NMR spectroscopy. Specifically, for a solution of **39a** in d_6-benzene, irradiation of the peak for the 21-H at 5.87 ppm enhanced the OMe resonance at 3.26 ppm and the pyrrolic 19-methyl unit. The 6-H signal at 5.61 ppm correlated to the 8^1-H benzo-proton at 7.88 ppm, and the 4-H peak at 6.97 ppm enhanced the C-3 resonance at 6.32 ppm and the bridge CH at 5.61 ppm. The 11-H *meso*-proton was identified as the peak at 6.67 ppm as this correlated with the ethyl CH_2's, while the 16-H *meso*-proton showed up at 7.13 ppm. Although this product was isolated in less than 7% yield, it is interesting to note that it was formed regio- and stereoselectively (i.e. only one diastereomer is formed, albeit in racemic form). However, once again it was not possible to tell whether the *cis*- or *trans*-isomer had been generated. The minor product derived from dimethoxy 23-carbabenziporphyrin **12d** was similarly identified as a single diastereomer **39b** with a hydroxyl substituent as C-6. The origin of the observed regioselectivity is not clear.

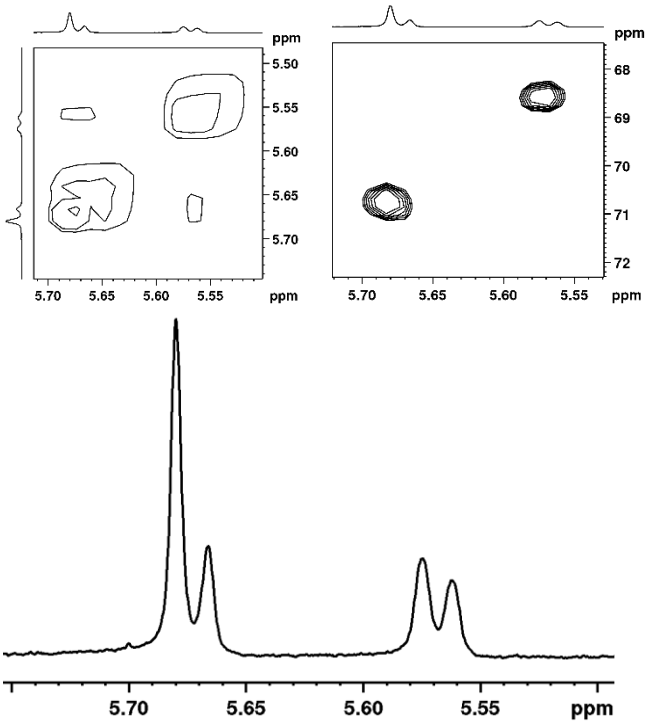

Figure 19. Partial proton NMR spectrum in d_6-DMSO of **39a** showing the CH-O and OH protons. Top left: ^{1}H-^{1}H COSY and top right: ^{1}H-^{13}C HSQC NMR spectra for the same region. The results show that the doublet at 5.57 ppm corresponds to the CH connected to the hydroxyl group, while the singlet at 5.68 is due to the CH-OMe. The latter resonance overlaps with the doublet due to the OH unit.

Conclusion

A series of methoxy- and dimethoxy benzocarbabenziporphyrins have been prepared by the acid catalyzed condensation of fulvene dialdehydes with dipyrrylmethane dicarboxylic acids. The presence of a methoxy-substituent introduces a degree of aromatic character that is further enhanced upon protonation or by the introduction of a second methoxy group. C-protonation occurs under strongly acidic conditions to give dicationic species that show pronounced aromatic ring currents. NICS calculations and AICD plots indicate that these characteristics are due, in part, to 23-atom 22π electron delocalization pathways through the fused benzo-units. These new

dicarbaporphyrinoid structures are stable for prolonged periods in the solid state or in solution. Reaction with silver(I) acetate in dichloromethane-methanol solutions failed to give metalated derivatives but instead selectively afforded nonaromatic oxidation products. The major products incorporate two additional methoxy substituents, but minor products were observed that regioselectively introduced a *meso*-hydroxy group. The results further demonstrate the unique reactivity and spectroscopic properties of *adj*-dicarbaporphyrinoid systems.

Experimental Section

Melting points are uncorrected. NMR spectra were recorded using a 400 or 500 MHz NMR spectrometer and were run at 302 K unless otherwise indicated. ^{1}H NMR values are reported as chemical shifts δ, relative integral, multiplicity (s, singlet; d, doublet; t, triplet; q, quartet; m, multiplet; br, broad peak) and coupling constant (*J*). Chemical shifts are reported in parts per million (ppm) relative to $CDCl_3$ (^{1}H residual $CHCl_3$ δ 7.26, ^{13}C $CDCl_3$ triplet δ 77.23) or DMSO-d_6 (^{1}H residual DMSO-d_5 pentet δ 2.49, ^{13}C DMSO-d_6 heptet δ 39.7), and coupling constants were taken directly from the spectra. NMR assignments were made with the aid of ^{1}H-^{1}H COSY, HSQC, DEPT-135, and NOE difference proton NMR spectroscopy. 2D experiments were performed by using standard software. High-resolution mass spectra (HRMS) were obtained by using a double focusing magnetic sector instrument. ^{1}H and ^{13}C NMR spectra for all new compounds are reported in Supporting Information.

1-(3-Iodo-4-methoxyphenylmethylene)indene-3-carbaldehyde (**24b**). Dibutylboron triflate (1.0 M in dichloromethane, 800 μL) was added to a stirred solution of 3-iodo-4-methoxybenzaldehyde (273 mg, 1.04 mmol) in dichloromethane (150 ml). A solution of indene enamine **16** (195.8 mg, 1.14 mmol) in dichloromethane (150 ml) was then added dropwise over

10 min, and the resultant solution stirred at room temperature overnight. Saturated sodium acetate solution (70 mL) was added and the mixture was allowed to stir for 10 min. The product was extracted with dichloromethane, washed with saturated sodium bicarbonate solution and then with brine. The organic phase was dried over sodium sulfate, the solvent removed under reduced pressure, and the residue purified by flash chromatography on silica gel eluting with 30% hexanes-dichloromethane. Recrystallization with chloroform-pentane gave the fulvene aldehyde (172 mg, 0.444 mmol, 43%) as a light orange powder, mp 154 °C, dec. ^{1}H NMR (500 MHz, $CDCl_3$): δ 3.97 (3H, s), 6.92 (1H, d, J = 8.5 Hz), 7.31-7.37 (2H, m), 7.63 (1H, dd, J = 2.2, 8.5 Hz), 7.66 (1H, s), 7.70-7.72 (1H, m), 8.09-8.11 (2H, m), 10.20 (1H, s). ^{13}C{^{1}H} NMR (125 MHz, $CDCl_3$): δ 56.8, 87.0, 111.2, 119.5, 123.1, 126.8, 128.2, 130.9, 132.5, 134.4, 137.3, 137.7, 137.8, 139.1, 141.8, 143.1, 159.7, 189.2. HRMS (EI) *m/z*: M^+ Calcd for $C_{18}H_{13}IO_2$ 387.9961; Found: 387.9957.

1-(3-Bromo-4-methoxyphenylmethylene)indene-3-carbaldehyde (**24a**). 3-Bromo-4-methoxybenzaldehyde (227 mg, 1.06 mmol) was reacted with indene enamine **16** (198 mg, 1.16 mmol) in the presence of dibutylboron triflate (1.0 M in dichloromethane, 800 μL) under the conditions described above. The crude product was purified by flash chromatography on silica gel eluting with 40% hexanes-dichloromethane. Recrystallization with chloroform-hexanes gave the fulvene aldehyde (223 mg, 0.654 mmol, 62%) as an orange powder, mp 173-174 °C. ^{1}H NMR (500 MHz, $CDCl_3$): δ 3.97 (3H, s), 6.99 (1H, d, J = 8.5 Hz), 7.30-7.36 (2H, m), 7.58 (1H, dd, J = 2.1, 8.5 Hz), 7.65 (1H, s), 7.66 (1H, s), 7.69-7.71 (1H, m), 7.86 (1H, d, J = 2.1 Hz), 8.08-8.10 (1H, m), 10.19 (1H, s). ^{13}C{^{1}H} NMR (125 MHz, $CDCl_3$): δ 56.7, 112.3, 112.8, 119.5, 123.0, 126.8, 128.2, 130.2, 131.6, 134.5, 135.5, 137.3, 137.2, 137.81, 137.82, 139.1, 143.1,

157.5, 189.2. HRMS (EI) *m/z*: M^+ Calcd for $C_{18}H_{13}BrO_2$ 340.0099; Found: 340.0103. Anal calcd for $C_{18}H_{13}BrO_2$: C, 63.36; H, 3.84. Found: C, 63.34; H, 3.57.

1-(5-Iodo-2,4-dimethoxyphenylmethylene)indene-3-carbaldehyde (**29**). *N*-Iodosuccinimide (95%, 308 mg, 1.30 mmol) was added to a stirred solution of fulvene **28**[32] (200 mg, 0.68 mmol) in dichloromethane (100 mL). Three drops of TFA were added and the mixture was refluxed overnight. The solution was washed with saturated sodium bicarbonate solution and the organic phase dried over sodium sulfate. The solvent was removed under reduced pressure, and the residue purified by flash chromatography on silica gel eluting with 30% hexanes-dichloromethane. Recrystallization from chloroform-pentane gave the fulvene aldehyde in approximately 96% purity (200 mg, 0.48 mmol, 70%) as bright orange crystals, mp 216-218 ºC, dec. ^{1}H NMR (500 MHz, $CDCl_3$): δ 3.95 (3H, s), 3.98 (3H, s), 6.47 (1H, s), 7.30-7.35 (2H, m), 7.62 (1H, d, *J* = 0.8 Hz), 7.75-7.77 (1H, m), 7.98 (1H, t, *J* = 0.8 Hz), 8.01 (1H, d, *J* = 0.6 Hz), 8.10-8.12 (1H, m), 10.21 (1H, s). ^{13}C{^{1}H} NMR (125 MHz, $CDCl_3$): 56.2, 56.8, 75.5, 95.4, 119.6, 120.5, 122.9, 126.6, 127.9, 130.5, 137.2, 137.3, 138.0, 139.7, 141.5, 142.5, 160.8, 161.1, 189.4. HRMS (EI) *m/z*: M^+ Calcd for $C_{19}H_{15}O_3I$: 418.0066. Found: 418.0072.

3-(Dimethoxymethyl)-1-(5-iodo-4-methoxyphenylmethylene)indene (**25b**). Fulvene **24b** (200 mg, 0.52 mmol), trimethyl orthoformate (5 mL), and dichloromethane (60 mL) were added to round-bottomed flask equipped with a drying tube. Cerium chloride heptahydrate (540 mg) and methanol (1600 mL) were added, and the contents of the flask were refluxed for 2 h. The reaction was quenched with saturated sodium bicarbonate solution (100 mL), and the product extracted with dichloromethane and dried over sodium sulfate. The solvent was evaporated under reduced pressure and the residue recrystallized from chloroform-hexanes to give the protected fulvene (195 mg, 0.40 mmol, 87%) as a yellow solid, mp 99-100 ºC. ^{1}H NMR (500 MHz,

$CDCl_3$): δ 3.39 (6H, s) 3.93 (3H, s), 5.55 (1H, d, *J* = 1.2 Hz), 6.88 (1H, d, *J* = 8.5 Hz), 7.06 (1H, br t, *J* = 1.0 Hz), 7.22-7.29 (2H, m), 7.35 (1H, s), 7.51-7.53 (1H, m), 7.63 (1H, dd, *J* = 2.2, 8.5 Hz), 7.65-7.67 (1H, m), 8.04 (1H, d, *J* = 2.2 Hz). $^{13}C\{^1H\}$ NMR (125 MHz, $CDCl_3$): δ 52.8, 56.7, 86.5, 100.3, 111.1, 119.1, 120.7, 124.2, 125.7, 127.4, 127.7, 131.7, 131.8, 138.0, 138.4, 139.8, 141.3, 144.3, 158.6. HRMS (EI) *m/z*: M^+ Calcd for $C_{20}H_{19}O_3I$: 434.0379. Found: 434.0378.

1-(3-Formyl-4-methoxyphenylmethylene)indene-3-carbaldehyde (**13**). A 2.0 M solution of *n*-butylmagnesium chloride in THF (0.58 mL) was added to ether (10 mL) in a 100 mL round bottom flask equipped with a thermometer, a drying tube and a rubber septum. After the solution had been cooled to 0 ºC, a 1.6 M solution of *n*-BuLi in hexanes (1.5 mL) was added, and the mixture stirred for 10 min at 0 ºC. The mixture was then cooled to -100 °C, and a solution of protected fulvene **25b** (100 mg, 0.23 mmol) in ether (20 mL) was added dropwise. The mixture was allowed to stir at -100 ºC for 45 min. DMF (0.5 mL) was added while maintaining the temperature at -100 °C, and the cooling bath was then removed and stirring continued for 2 h. The reaction was quenched by the addition of 10% HCl, and washed with saturated ammonium chloride solution. The product was extracted with dichloromethane, dried over sodium sulfate and the solvent removed under reduced pressure. The residue was purified by flash chromatography on silica eluting with dichloromethane. Recrystallization with chloroform-hexanes gave the fulvene dialdehyde (38 mg, 0.13 mmol, 56%) as a bright orange solid, mp 188 ºC. ^1H NMR (500 MHz, $CDCl_3$): δ 4.04 (3H, s), 7.14 (1H, d, *J* = 8.7 Hz), 7.32-7.37 (2H, m), 7.68 (1H, br d, *J* = 0.8 Hz), 7.72-7.74 (1H, m), 7.75 (1H, br q, *J* = 0.5 Hz), 7.86 (1H, dd, *J* = 2.4, 8.7 Hz), 8.09-8.11 (1H, m), 8.15 (1H, d, *J* = 2.4 Hz), 10.20 (1H, s), 10.52 (1H, s). $^{13}C\{^1H\}$ NMR (125 MHz, $CDCl_3$): δ 56.3, 112.8, 119.5, 123.1, 125.5, 126.9, 128.3, 129.1, 130.9, 134.6, 137.4,

137.8, 138.0, 138.2, 139.0, 143.3, 162.9, 189.2, 189.3. HRMS (EI) *m/z*: M^+ Calcd for $C_{19}H_{14}O_3$ 290.0943; Found: 290.0941.

1-(5-Formyl-2,4-dimethoxyphenylmethylene)indene-3-carbaldehyde (**14**). Fulvene **29** (200 mg, 0.478 mmol), trimethyl orthoformate (5 mL), and cerium chloride heptahydrate (540 mg) were reacted under the same conditions used to prepare **13**. Recrystallization from chloroform-hexanes gave the crude protected fulvene **30** (187 mg, 0.402 mmol, 84%) as a yellow solid. Acetal **30** (100 mg, 0.22 mmol) was converted into the corresponding dialdehyde using the conditions described above. The crude product was purified by flash chromatography on silica eluting with dichloromethane. Recrystallization from chloroform-hexanes gave the fulvene dialdehyde in ca. 96% purity (46 mg, 0.14 mmol, 67%) as a bright orange solid, mp 206-208 ºC. ^{1}H NMR (500 MHz, $CDCl_3$): δ 4.03 (3H, s), 4.04 (3H, s), 6.51 (1H, s), 7.30-7.36 (2H, m), 7.64 (1H, d, *J* = 0.7 Hz), 7.75-7.77 (1H, m), 7.99 (1H, br t, *J* = 0.7 Hz), 8.10-8.12 (1H, m), 8.14 (1H, d, *J* = 0.7 Hz), 10.19 (1H, s), 10.38 (1H, s). ^{13}C{^{1}H} NMR (125 MHz, $CDCl_3$): δ 56.2, 56.4, 94.5, 118.9, 119.2, 119.7, 123.0, 126.6, 128.1, 130.4, 132.4, 137.5, 137.8, 138.1, 139.9, 142.8, 164.9, 165.4, 188.0, 189.5. HRMS (EI) *m/z*: M^+ Calcd for $C_{20}H_{16}O_4$ 320.1049; Found: 320.1048.

14,18-Diethyl-2-methoxy-13,19-dimethyl-23-carbabenzo[*h*]benziporphyrin (**12a**). Dipyrrylmethane dicarboxylic acid **15a** (33 mg, 0.10 mmol) was stirred with 5 mL of TFA under nitrogen for 2 min. The solution was diluted with dichloromethane (100 mL) and fulvene dialdehyde **13** (30 mg, 0.10 mmol) in 50 mL of dichloromethane was added immediately. The solution was stirred under nitrogen at room temperature overnight. The solution was washed with water and saturated sodium bicarbonate solution, and the solvent was removed under reduced pressure. The residue was purified by column chromatography on grade 3 alumina eluting with dichloromethane. Recrystallization from chloroform-hexanes gave the benzicarbaporphyrin (35

mg, 0.072 mmol, 70%) as a fluffy green solid, mp 230 ºC, dec. UV-Vis ($CHCl_3$): λ_{max} ($\log_{10}$ ε) 342 (4.74), 415 (4.66), 654 nm (3.78). UV-vis (1% TFA-$CHCl_3$): λ_{max} ($\log_{10}$ ε) 342 (4.83), 415 (4.37), 474 (4.33), 565 (4.05), 609 (4.06), 695 nm (3.92). UV-vis (TFA): λ_{max} ($\log_{10}$ ε) 319 (4.57), 395 (4.87), 482 (4.25), 674 (4.42), 774 nm (3.95). ^{1}H NMR (500 MHz, $CDCl_3$): δ 1.29 (3H, t, *J* = 7.6 Hz), 1.33 (3H, t, *J* = 7.6 Hz) (2 x CH_2CH_3), 2.49 (6H, s, 13,19-Me), 2.82 (2H, q, *J* = 7.6 Hz) 2.86 (2H, q, *J* = 7.6 Hz) (2 x CH_2CH_3), 4.12 (3H, s, OMe), 4.97 (1H, s, 23-H), 6.03 (1H, d, *J* = 2.2 Hz, 22-H), 6.53 (1H, s, 16-H), 7.08 (1H, s, 11-H), 7.24 (1H, d, *J* = 8.5 Hz, 3-H), 7.36-7.43 (2H, m, 8^2,9^2-H), 7.81 (1H, d, *J* = 7.4 Hz, 9^1-H), 7.87 (1H, s, 6-H), 7.90 (1H, s, 21-H), 7.97-8.01 (2H, m, 4-H and 8^1-H). ^{13}C{^{1}H} NMR (125 MHz, $CDCl_3$): δ 10.2 (Me), 10.8 (Me), 15.5 (2 x CH_2CH_3), 18.2 (CH_2CH_3), 18.6 (CH_2CH_3), 56.3 (OMe), 89.4 (16-CH), 98.3 (11-CH), 111.2 (21-CH), 111.4 (3-CH), 118.9 (9^1-CH), 119.1 (22-CH), 119.4 (8^1-CH), 122.4 (23-CH), 123.4, 124.1, 125.8, 127.0 (8^2-CH), 127.9 (9^2-CH), 136.1 (4-CH), 137.0, 138.1, 139.0, 139.28, 139.32, 140.4, 141.4, 142.1, 147.0, 152.2, 153.8, 160.8, 166.3. ^{1}H NMR (500 MHz, 1 drop TFA-$CDCl_3$): δ 1.33 (3H, t, *J* = 7.7 Hz), 1.35 (3H, t, *J* = 7.7 Hz) (2 x CH_2CH_3), 2.63 (3H, s), 2.64 (3H, s) (13,19-Me), 2.94-2.99 (4H, m, 2 x CH_2CH_3), 4.17 (3H, s, OMe), 4.34 (1H, br s, 23-H), 4.35 (1H, s, 22-H), 5.42 (1H, br s, NH), 5.87 (1H, br s, NH), 6.84 (1H, s, 16-H), 7.35 (1H, d, *J* = 8.7 Hz), 7.43-7.49 (2H, m, 8^2,9^2-H), 7.72 (1H, s, 11-H), 7.78 (1H, d, *J* = 7.2 Hz, 9^1-H), 7.96 (1H, d, *J* = 7.2 Hz, 8^1-H), 8.08 (1H, s, 21-H), 8.19 (1H, dd, *J* = 2.0, 8.7 Hz), 8.20 (1H, s, 6-H). ^{13}C{^{1}H} NMR (125 MHz, trace TFA-$CDCl_3$): δ 10.4, 10.9, 14.8, 14.9, 18.3, 18.4, 56.7, 87.7, 108.7, 111.8, 112.8, 115.0, 119.3, 119.8, 122.4, 126.6, 127.6, 127.9, 128.2, 129.4, 138.5, 138.8, 138.9, 140.10, 140.12, 140.2, 140.4, 140.9, 142.8, 143.7, 144.5, 153.9, 157.7, 162.6. ^{1}H NMR (500 MHz, TFA): δ 1.10 (2H, s, 23-CH_2), 1.94 (3H, t, *J* = 7.7 Hz), 2.03 (3H, t, *J* = 7.7 Hz) (2 x CH_2CH_3), 3.28 (1H, s, 22-H), 3.42 (3H, s), 3.49 (3H, s) (13,19-Me), 3.80-3.90 (4H, m, 2 x

C*H*$_2$CH$_3$), 4.92 (3H, s, OMe), 8.15 (1H, d, *J* = 8.9 Hz), 8.60 (1H, t, *J* = 7.6 Hz), 8.83 (1H, t, *J* = 7.6 Hz), 9.03 (1H, s), 9.21 (1H, br d, *J* = 9.0 Hz), 9.37 (1H, d, *J* = 8.1 Hz), 9.44 (1H, s), 9.47 (1H, d, *J* = 8.1 Hz), 9.54 (1H, s), 10.38 (1H, s). HRMS (EI) *m/z*: M^+ Calcd for $C_{34}H_{32}N_2O$: 484.2515; Found: 484.2518. Anal calcd for $C_{34}H_{32}N_2O$: C, 84.19; H, 6.65; N, 5.78. Found: C, 84.28; H, 6.72; N, 5.88.

2-Methoxy-13,14,18,19-tetramethyl-23-carbabenzo[*h*]benziporphyrin (**12b**). Dipyrrylmethane dicarboxylic acid **15b** (30 mg, 0.103 mmol) and fulvene dialdehyde **13** (30 mg, 0.103 mmol) were reacted under the previously described conditions. Recrystallization from chloroform-hexanes gave the benzicarbaporphyrin (32 mg, 0.070 mmol, 68%) as a fluffy green solid, mp >300 ºC. UV-Vis (1% Et_3N-$CHCl_3$): λ_{max} ($\log_{10}$ ε) 341 (4.73), 415 (4.67), 652 nm (3.78). UV-vis (1% TFA-$CHCl_3$): λ_{max} ($\log_{10}$ ε) 341 (4.82), 415 (4.37), 472 (4.32), 563 (4.03), 607 (4.04), 700 nm (3.90). UV-vis (TFA): λ_{max} ($\log_{10}$ ε) 319 (4.53), 394 (4.86), 482 (4.22), 673 (4.41), 775 nm (3.92). ^{1}H NMR (500 MHz, $CDCl_3$): δ 2.37 (3H, s), 2.40 (3H, s), 2.470 (3H, s), 2.474 (3H, s) (13,14,18,19-Me), 4.11 (3H, s, OMe), 4.97 (1H, s, 23-H), 6.05 (1H, d, *J* = 2.2 Hz, 22-H), 6.47 (1H, s, 16-H), 7.05 (1H, s, 11-H), 7.23 (1H, d, *J* = 8.5 Hz, 3-H), 7.36-7.43 (2H, m, 8^2,9^2-H), 7.81 (1H, d, *J* = 7.2 Hz, 9^1-H), 7.86 (1H, s, 6-H), 7.88 (1H, s, 21-H), 7.97-8.00 (2H, m, 4-H and 8^1-H). ^{1}H NMR (500 MHz, TFA-$CDCl_3$): δ 2.48 (3H, s), 2.49 (3H, s), 2.58 (3H, s), 2.59 (3H, s) (13,14,18,19-Me), 4.16 (3H, s, OMe), 4.29 (1H, br d, *J* = 2 Hz, 22-H), 4.31 (1H, br s, 23-H), 5.32 (1H, br s, NH), 5.83 (1H, br s, NH), 6.76 (1H, s, 16-H), 7.32 (1H, d, *J* = 8.6 Hz), 7.40-7.47 (2H, m, 8^2,9^2-H), 7.63 (1H, s, 11-H), 7.73-7.75 (1H, m, 9^1-H), 7.90-7.92 (1H, m, 8^1-H), 8.01 (1H, s, 21-H), 8.12 (1H, s, 6-H), 8.14 (1H, dd, *J* = 2.1, 8.6 Hz). ^{13}C{^{1}H} NMR (125 MHz, trace TFA-$CDCl_3$): δ 10.1, 10.2, 10.6, 11.2, 56.9, 87.5, 108.8, 112.0, 112.4, 113.4, 119.6, 120.0, 122.0, 127.1, 127.7, 127.97, 128.03, 128.1, 134.5, 134.9, 138.2, 138.91, 138.97, 140.0, 140.2, 142.2,

142.4, 144.0, 145.8, 155.0, 158.7, 162.2. ^{1}H NMR (500 MHz, TFA, 50 ºC): δ 0.69 (2H, s, 23-CH_2). 2.88 (1H, s, 22-H), 2.91 (3H, s), 2.98 (6H, s), 3.05 (3H, s) (4 x Me), 4.34 (1H, v br, NH), 4.50 (3H, s, OMe), 7.73 (1H, d, *J* = 8.7 Hz, 3-H), 8.19 (1H, br t, *J* = 7.2 Hz), 8.41 (1H, br t, *J* = 7.2 Hz), 8.59 (1H, s), 8.78 (1H, d, *J* = 8.5 Hz), 8.96 (1H, d, *J* = 7.7 Hz), 9.02 (1H, s), 9.05 (1H, d, *J* = 8.5 Hz), 9.11 (1H, s), 9.95 (1H, s). HRMS (EI) *m/z*: M^+ Calcd for $C_{32}H_{28}N_2O$ 456.2202; Found 456.2207. Anal calcd for $C_{32}H_{28}N_2O$: C, 84.18; H, 6.18; N, 6.14. Found: C, 83.78; H, 5.96; N, 6.21.

2-Methoxy-14,18-(2-methoxycarbonylethyl)-13,19-dimethyl-23-carbabenzo[*h*]benziporphyrin (**12c**). Dipyrrylmethane dicarboxylic acid **15c** (45 mg, 0.103 mmol) was condensed with fulvene dialdehyde **13** (30 mg, 0.103 mmol) by the procedure described above. Recrystallization from chloroform-hexanes gave the benzicarbaporphyrin (39 mg, 0.065 mmol, 63%) as a fluffy green solid, mp > 300 ºC. UV-Vis (1% Et_3N-$CHCl_3$): λ_{max}/nm ($\log_{10}$ ε) 343 (4.73), 417 (4.62), 655 (3.76). UV-vis (1% TFA-$CHCl_3$): λ_{max} ($\log_{10}$ ε) 343 (4.82), 419 (4.35), 474 (4.32), 567 (4.05), 610 (4.07), 700 nm (3.89). UV-vis (TFA): λ_{max} ($\log_{10}$ ε) 322 (4.52), 399 (4.85), 492 (4.21), 679 nm (4.38). ^{1}H NMR (500 MHz, $CDCl_3$): δ 2.51 (6H, s, 13,19-Me), 2.69 (2H, t, *J* = 7.8 Hz), 2.73 (2H, t, *J* = 7.7 Hz) (2 x C*H*$_2$$CO_2$Me), 3.14-3.20 (4H, m, 14,18-CH_2), 3.689 (3H, s), 3.692 (3H, s) (2 x ester OMe), 4.11 (3H, s, OMe), 4.87 (1H, br s, 23-H), 5.90 (1H, br d, *J* = 2.0 Hz, 22-H), 6.51 (1H, s, 16-H), 7.10 (1H, s, 11-H), 7.23 (1H, d, *J* = 8.6 Hz, 3-H), 7.36-7.43 (2H, m, 8^2,9^2-H), 7.79-7.81 (1H, m, 9^1-H), 7.87 (1H, s, 6-H), 7.92 (1H, s, 21-H), 7.96-7.98 (1H, m, 8^1-H), 7.99 (1H, dd, *J* = 2.3, 8.6 Hz, 4H). ^{13}C{^{1}H} NMR (125 MHz, $CDCl_3$): δ 10.4 (Me), 11.0 (Me), 20.3 (CH_2), 20.7 (CH_2), 34.9 (CH_2), 35.0 (CH_2), 51.94 (ester OMe), 52.00 (ester OMe), 56.3 (OMe), 89.1 (16-CH), 99.1 (11-CH), 111.5 (21-CH), 111.9 (3-CH), 118.9 (9^1-CH), 119.1 (22-CH), 119.4 (8^1-CH), 122.8 (23-CH), 123.7, 123.9, 125.9, 127.0

(8^2-CH), 127.9 (9^2-CH), 135.2 (4-CH), 136.7, 137.4, 137.8, 138.1, 139.15, 139.21, 141.9, 143.3, 161.0, 173.4, 173.6. ^{1}H NMR (500 MHz, 1 drop TFA-$CDCl_3$): δ 2.65 (6H, s, 13,19-Me), 2.77-2.82 (4H, 2 overlapping triplets, 2 x CH_2CO2Me), 3.30 (4H, t, J = 7.5 Hz, 14,18-CH_2), 3.699 (3H, s), 3.701 (3H, s) (2 x ester OMe), 4.17 (3H, s, OMe), 4.36 (1H, br d, J = 2.0 Hz, 22-H), 4.46 (1H, s, 23-H), 5.70 (1H, br s, NH), 6.36 (1H, br s, NH), 7.00 (1H, s, 16-H), 7.33 (1H, d, J = 8.7 Hz), 7.43-7.49 (2H, m, 8^2,9^2-H), 7.76 (1H, s, 11-H), 7.78-7.80 (1H, m, 9^1-H), 7.96-7.98 (1H, m, 8^1-H), 8.10 (1H, s, 21-H), 8.19 (1H, dd, J = 2.0, 8.7 Hz), 8.22 (1H, s, 6-H). ^{13}C{^{1}H} NMR (125 MHz, trace TFA-$CDCl_3$): δ 10.7, 11.2, 20.0, 20.1, 34.0, 34.1, 52.6, 56.9, 87.5, 109.8, 112.3, 113.2, 113.5, 119.7, 120.1, 122.0, 127.2, 128.1, 128.21, 128.25, 128.9, 136.6, 136.8, 138.4, 138.9, 139.2, 140.3, 140.5, 142.0, 143.2, 143.7, 146.5, 153.8, 157.5, 162.6, 174.4. ^{1}H NMR (500 MHz, TFA): δ 0.95 (2H, s, 23-CH_2), 3.08 (1H, s, 22-H), 3.46 (3H, s), 3.52 (3H, s) (13,19-Me), 3.46-3.53 (4H, m, 2 x CH_2CO_2Me), 4.23-4.29 (4H, m, 14,18-CH_2), 4.27 (6H, s, 2 x ester OMe), 4.93 (3H, s, OMe), 8.12 (1H, d, J = 8.9 Hz), 8.63 (1H, t, J = 7.6 Hz), 8.86 (1H, t, J = 7.6 Hz), 9.03 (1H, s), 9.26 (1H, br d, J = 9.0 Hz), 9.34 (1H, s), 9.41 (1H, d, J = 8.1 Hz), 9.51-9.52 (2H, overlapping d and s), 9.60 (1H, s), 10.44 (1H, s). HRMS (ESI) *m/z*: $[M + H]^+$ Calcd for $C_{38}H_{37}N_2O_5$ 601.2702; Found 601.2707.

14,18-Diethyl-2,4-dimethoxy-13,19-dimethyl-23-carbabenzo[*h*]benziporphyrin (**12d**). Dipyrrylmethane **15a** (30.0 mg, 0.0943 mmol) was reacted with fulvene dialdehyde **14** (30.0 mg, 0.0927 mmol) under the previous conditions. Recrystallization from chloroform-hexanes gave the dimethoxybenzicarbaporphyrin (24.3 mg, 0.0473 mmol, 51%) as dark purple crystals, mp >300 ºC. UV-Vis ($CHCl_3$): λ_{max} ($\log_{10}$ ε) 345 (4.55), 432 (4.54), 618 nm (3.77). UV-vis (1% TFA-$CHCl_3$): λ_{max} ($\log_{10}$ ε) 348 (4.61), 432 (4.36), 483 (4.25), 630 nm (4.22). UV-vis (25% TFA-$CHCl_3$): λ_{max} ($\log_{10}$ ε) 328 (4.45), 358 (4.50), 413 (4.83), 477 (4.27), 702 nm (4.33). UV-vis

(TFA): λ_{max} ($\log_{10}$ ε) 325 (4.46), 354 (4.47), 409 (4.82), 476 (4.23), 697 (4.32), 724 (infl, 4.21), 798 nm (4.00). ^{1}H NMR (500 MHz, $CDCl_3$): δ 1.32 (3H, t, *J* = 7.6 Hz), 1.37 (3H, t, *J* = 7.6 Hz) (2 x CH_2CH_3), 2.57 (3H, s), 2.58 (3H, s), 2.91 (2H, q, *J* = 7.6 Hz), 2.96 (2H, q, *J* = 7.6 Hz) (14,18-CH_2), 3.85 (1H, s, 23-H), 4.17 (3H, s), 4.18 (3H, s) (2 x OMe), 4.89 (1H, br s, 22-H), 6.77 (2H, s, 3,16-H), 7.26 (1H, s, 11-H), 7.37-7.44 (2H, m, 8^2,9^2-H), 7.88 (1H, d, *J* = 7.4 Hz, 9^1-H), 8.08-8.10 (2H, m, 8^1,21-H), 8.60 (1H, s, 6-H). ^{1}H NMR (500 MHz, CD_2Cl_2): δ 1.34 (3H, t, *J* = 7.6 Hz), 1.40 (3H, t, *J* = 7.6 Hz) (2 x CH_2CH_3), 2.59 (3H, s), 2.62 (3H, s), 2.95 (2H, q, *J* = 7.6 Hz), 3.01 (2H, q, *J* = 7.6 Hz) (14,18-CH_2), 3.52 (1H, s, 23-H), 4.21 (3H, s), 4.22 (3H, s) (2 x OMe), 4.62 (1H, br s, 22-H), 6.86 (1H, s, 3-H), 6.87 (1H, s, 16-H), 7.35 (1H, s, 11-H), 7.40-7.47 (2H, m, 8^2,9^2-H), 7.94 (1H, d, *J* = 7.2 Hz, 9^1-H), 8.12 (1H, d, *J* = 7.1 Hz, 8^1-H), 8.18 (1H, s, 21-H), 8.68 (1H, s, 6-H). ^{1}H NMR (500 MHz, 1 drop TFA-$CDCl_3$): δ 1.37 (3H, t, *J* = 7.6 Hz), 1.43 (3H, t, *J* = 7.6 Hz) (2 x CH_2CH_3), 2.19 (1H, s), 2.34 (1H, s), 2.75 (3H, s), 2.76 (3H, s) (13,19-Me), 3.09-3.16 (4H, m, 2 x CH_2CH_3), 3.19 (1H, br s, NH), 3.86 (1H, br s, NH), 4.26 (6H, s, 2 x OMe), 6.86 (1H, s, 3-H), 7.26 (1H, s, 16-H), 7.40-7.46 (2H, m, 8^2,9^2-H), 7.81 (1H, d, *J* = 7.2 Hz, 9^1-H), 7.96 (1H, s, 11-H), 8.01 (1H, d, *J* = 7.2 Hz, 8^1-H), 8.45 (1H, s, 21-H), 8.83 (1H, s, 6-H). ^{13}C{^{1}H} NMR (125 MHz, 1 drop TFA-$CDCl_3$): δ 10.6, 11.1, 15.0, 15.2, 18.5, 18.6, 57.1, 57.2, 86.9, 96.4, 106.4, 112.5, 112.7, 115.1, 118.5, 119.6, 120.20, 120.23, 124.3, 126.9, 127.6, 137.4, 137.8, 138.6, 139.4, 139.7, 139.9, 140.46, 140.49, 143.0, 144.7, 150.8, 154.5, 166.3, 168.4. ^{1}H NMR (500 MHz, TFA): δ -0.72 (2H, s, 23-CH_2), 1.18 (1H, s, 22-H), 1.98 (3H, t, *J* = 7.7 Hz), 2.09 (3H, t, *J* = 7.7 Hz) (2 x CH_2CH_3), 3.10 (1H, br s, NH), 3.59 (3H, s), 3.60 (3H, s) (13,18-Me), 3.95 (1H, br s, NH), 3.99-4.08 (4H, m, 2 x CH_2CH_3), 5.04 (3H, s), 5.09 (3H, s) (2 x OMe), 7.69 (1H, s, 3-H), 8.75 (1H, t, *J* = 7.6 Hz), 8.92 (1H, t, *J* = 7.6 Hz) (8^2,9^2-H), 9.57 (1H, s, 16-H), 9.67 (1H, d, *J* = 8.1 Hz), 9.74 (1H, d, *J* = 8.1 Hz), 10.07 (1H, s, 11-H), 10.56 (1H, s, 6-H), 10.72

(1H, s, 21-H). HRMS (EI) *m/z*: Calcd for $C_{35}H_{34}N_2O_2$ 514.2620; Found: 514.2616. HRMS (ESI) *m/z*: $[M + H]^+$ Calcd for $C_{35}H_{35}N_2O_2$ 515.2699; Found 515.2688.

2,4-Dimethoxy-13,14,18,19-tetramethyl-23-carbabenzo[*h*]benziporphyrin (**12e**). Dipyrrylmethane **15b** (27.2 mg, 0.0938 mmol) was reacted with fulvene dialdehyde **14** (30.0 mg, 0.0937 mmol) under the previous conditions. Recrystallization from chloroform-hexanes gave the dimethoxybenzicarbaporphyrin (27.3 mg, 0.0562 mmol, 60%) as a black solid, mp >300 ºC. UV-Vis (1% Et_3N-CH_2Cl_2): λ_{max}/nm ($\log_{10}$ ε) 343 (4.62), 431 (4.63), 582 (sh, 3.81), 621 (3.83), 681 (sh, 3.55). UV-Vis (1% TFA-CH_2Cl_2): λ_{max}/nm ($\log_{10}$ ε) 348 (4.63), 435 (4.44), 482 (4.26), 582 (sh, 3.95), 633 (4.22), 675 (sh, 4.05), 734 (sh, 3.92). UV-Vis (TFA): λ_{max}/nm ($\log_{10}$ ε) 326 (4.43), 356 (4.50), 408 (4.87), 477 (4.24), 696 (4.36), 724 (sh, 4.27), 796 (4.04). ^{1}H NMR (500 MHz, $CDCl_3$): δ 2.45 (3H, s), 2.50 (3H, s), 2.55 (3H, s), 2.56 (3H, s), 3.89 (1H, br s, 23-H), 4.16 (3H, s), 4.18 (3H, s) (2 x OMe), 4.94 (1H, br s, 22-H), 6.71 (2H, s, 3-H), 6.77 (1H, s, 16-H), 7.24 (1H, s, 11-H), 7.37-7.44 (2H, m, 8^2,9^2-H), 7.87 (1H, d, *J* = 7.2 Hz, 9^1-H), 8.06 (1H, s, 21-H), 8.09 (1H, d, 8^1-H), 8.60 (1H, s, 6-H). ^{1}H NMR (500 MHz, trace TFA-$CDCl_3$): δ 2.57 (3H, s), 2.61 (3H, s), 2.67 (3H, s), 2.69 (3H, s) (4 x Me), 3.06 (1H, br s, 23-H), 3.46 (1H, br s, 22-H), 4.21 (3H, s), 4.22 (3H, s) (2 x OMe), 6.77 (1H, s, 3-H), 7.05 (1H, s, 16-H), 7.40-7.47 (2H, m, 8^2,9^2-H), 7.86-7.88 (1H, m, 9^1-H), 7.88 (1H, s, 11-H), 8.08 (1H, d, *J* = 7.2 Hz, 8^1-H), 8.30 (1H, s, 21-H), 8.87 (1H, s, 6-H). ^{1}H NMR (500 MHz, TFA): δ -1.11 (1H, s, 23-CH_2), 0.74 (1H, s, 22-H), 3.01 (3H, s), 3.10 (9H, s) (4 x Me), 4.56 (3H, s), 4.62 (3H, s) (2 x OMe), 7.13 (1H, s, 3-H), 8.31 (1H, t, *J* = 7.5 Hz, 9^2-H), 8.48 (1H, t, *J* = 7.5 Hz, 8^2-H), 9.00 (1H, s), 9.21 (1H, d, *J* = 8.2 Hz), 9.26 (1H, d, *J* = 8.2 Hz), 9.50 (1H, s, 11-H), 10.00 (1H, s, 6-H), 10.13 (1H, s, 21-H). ^{13}C{^{1}H} NMR (125 MHz, TFA): δ 10.5, 10.7, 10.9, 11.6, 37.1 (23-CH_2), 58.7 (OMe), 58.9 (OMe), 97.7 (3-CH), 105.5 (11-CH), 106.2 (16-CH), 116.5 (6-CH), 118.8, 121.8 (22-CH), 122.5, 123.4 (8^1-

CH), 125.2 (9^1-H), 128.6 (21-CH), 131.8 (9^2-CH), 137.2 (8^2-CH), 137.8, 138.7, 139.8, 140.4, 142.3, 144.6, 145.8, 149.0, 149.4, 151.7, 158.2, 165.0, 175.4, 177.4. HRMS (EI) *m/z*: M^+ Calcd for $C_{33}H_{30}N_2O_2$ 486.2307; Found 486.3295.

2,4-Dimethoxy-14,18-bis(2-methoxycarbonylethyl)-13,19-dimethyl-23-carbabenzo[*h*]benziporphyrin (**12f**). Dipyrrylmethane **15c** (40.7 mg, 0.0938 mmol) was reacted with fulvene dialdehyde **14** (30.0 mg, 0.0937 mmol) under the previous conditions. Recrystallization from chloroform-hexanes gave the dimethoxybenzicarbaporphyrin (30.7 mg, 0.0487 mmol, 52%) as a green solid, mp >300 ºC. UV-Vis (1% Et_3N-CH_2Cl_2): λ_{max}/nm ($\log_{10}\varepsilon$) 345 (4.65), 432 (4.65), 582 (sh, 3.85), 624 (3.87), 686 (sh, 3.56). UV-Vis (1% TFA-CH_2Cl_2): λ_{max}/nm ($\log_{10}\varepsilon$) 352 (4.64), 438 (4.47), 485 (sh, 4.25), 582 (sh, 3.97), 637 (4.28), 684 (sh, 4.13), 746 (sh, 3.89). UV-Vis (TFA): λ_{max}/nm ($\log_{10}\varepsilon$) 327 (4.43), 412 (4.91), 488 (sh, 4.24), 698 (4.36), 805 (4.05). ^{1}H NMR (500 MHz, $CDCl_3$): δ 2.57 (3H, s, 19-Me), 2.60 (3H, s, 13-Me), 2.72 (2H, t, *J* = 7.8 Hz, 18-CH_2CH_2), 2.77 (2H, t, *J* = 7.8 Hz, 14-CH_2CH_2), 3.24 (2H, t, *J* = 7.8 Hz, 18-CH_2), 3.28 (2H, t, *J* = 7.8 Hz, 14-CH_2), 3.64 (1H, s, 23-H), 3.689 (3H, s), 3.694 (3H, s) (2 x ester OMe), 4.09 (3H, s), 4.11 (3H, s) (2 x OMe), 4.64 (1H, br s, 22-H), 6.57 (1H, br s, NH), 6.67 (1H, s, 3-H), 6.74 (1H, s, 16-H), 7.29 (1H, s, 11-H), 7.38-7.41 (2H, m, 8^2,9^2-H), 7.87 (1H, d, *J* = 7.2 Hz, 9^1-H), 8.08 (1H, d, *J* = 7.2 Hz, 8^1-H), 8.09 (1H, s, 21-H), 8.58 (1H, s, 6-H). ^{13}C{^{1}H} NMR (125 MHz, $CDCl_3$): δ 10.5 (13-Me), 11.2 (19-Me), 20.4 (14-CH_2), 20.9 (18-CH_2), 35.1 (14-CH_2CH_2), 35.3 (18-CH_2CH_2), 51.9, 52.0, 56.3, 56.4, 89.1 (16-CH), 95.0 (3-CH), 97.4 (11-CH), 112.7 (21-CH), 116.1 (6-CH), 116.9, 117.8, 118.9 (9^1-CH), 119.6 (8^1-CH), 120.0 (22-CH), 120.6 (23-CH), 125.7, 126.7, 134.8, 136.2, 136.9, 138.4, 139.7, 141.7, 143.3, 144.9, 149.1, 152.3, 163.7, 164.7, 165.0, 173.4 (C=O), 173.7 (C=O). ^{1}H NMR (500 MHz, 50% TFA-$CDCl_3$): δ -1.24 (2H, s, 23-CH_2), 0.57 (1H, s, 22-H), 3.00 (2H, t, *J* = 7.7 Hz), 3.08 (2H, t, *J* = 7.7 Hz),

3.16 (3H, s), 3.17 (3H, s) (2 x Me), 3.91-3.98 (4H, 2 overlapping triplets, 2 x CH_2CO), 4.60 (3H, s), 4.66 (3H, s) (2 x OMe), 7.16 (1H, s, 3-H), 8.35 (1H, t, J = 7.6 Hz), 8.52 (1H, t, J = 7.6 Hz) (8^2,9^2-H), 9.26 (1H, d, J = 8.2 Hz), 9.31 (1H, d, J = 8.4 Hz) (8^1,9^1-H), 9.32 (1H, s, 16-H), 9.58 (1H, s, 11-H), 10.07 (1H, s, 6-H), 10.21 (1H, s, 21-H). HRMS (ESI) *m/z*: $[M + H]^+$ Calcd for $C_{39}H_{39}N_2O_6$ 631.2808; Found 631.2801.

14,18-Diethyl-6,21-dihydro-2,6,21-trimethoxy-13,19-dimethyl-23-carbabenzo[*h*]benziporphyrin (**38a**). A suspension of silver(I) acetate (75 mg, 0.45 mmol) in methanol (25 mL) was added to a stirred solution of dicarbaporphyrin **12a** (21.3 mg, 0.044 mmol) in dichloromethane (25 mL), and the resulting mixture was stirred in the dark for 3 h at room temperature. The solution was washed with water and brine, back-extracting each time with dichloromethane, and the organic solutions were evaporated under reduced pressure. The residue was purified on a grade 3 alumina column, eluting with 50:50 dichloromethane−hexanes. A green band corresponding to a small amount of unreacted **12a** eluted first, followed by a dark purple fraction. This fraction was further purified by chromatography on a grade 3 alumina column, eluting with 50:50 dichloromethane−hexanes. Following evaporation of the solvent on a rotary evaporator and drying in vacuo overnight, the title compound (10.8 mg, 0.0197 mmol, 45%) was obtained as a dark purple solid, mp 219-221 °C. UV-Vis (CH_2Cl_2): λ_{max}/nm ($\log_{10}$ ε) 342 (4.44), 549 (sh, 4.41), 578 (4.45). ^{1}H NMR (500 MHz, $CDCl_3$): δ 1.10 (3H, t, J = 7.6 Hz), 1.15 (3H, t, J = 7.6 Hz) (2 x CH_2CH_3), 2.12 (3H, s, 13-Me), 2.20 (3H, s, 19-Me), 2.50-2.62 (4H, m, 14,18-CH_2), 3.41 (3H, s, 21-OMe), 3.43 (3H, s, 6-OMe), 3.75 (3H, s, 2-OMe), 5.20 (1H, br s, 6-H), 5.73 (1H, s, 21-H), 6.66 (1H, s, 16-H), 6.77 (1H, d, J = 8.1 Hz, 3-H), 6.92 (1H, br s, 23-H), 7.12 (1H, t, J = 0.7 Hz, 11-H), 7.21 (1H, dt, J = 1.1, 7.5 Hz, 9^2-H), 7.24 (1H, dd, J = 2.2, 8.1 Hz, 4-H), 7.29 (1H, dt, J = 1.1, 7.5 Hz, 8^2-H), 7.59 (1H, dt, J = 0.9, 7.4 Hz, 8^1-H), 7.65 (1H, dt, J =

0.9, 7.4 Hz, 9^1-H), 8.20 (1H, d, *J* = 2.2 Hz, 22-H), 11.13 (1H, br s, NH). $^{13}C\{^1H\}$ NMR (125 MHz, $CDCl_3$): δ 9.5 (19-Me), 9.6 (13-Me), 16.39, 16.46, 17.9, 18.3, 55.6 (2-OMe), 56.5 (6-OMe), 57.4 (21-OMe), 72.1 (21-CH), 80.0 (6-CH), 109.5 (3-CH), 115.8 (11-CH), 116.4 (16-CH), 119.2, 120.8, 125.2, 127.0, 127.1, 127.2, 127.4, 128.2, 128.9, 130.9, 131.1, 137.5, 139.0, 139.8, 141.6, 141.7, 142.5, 147.3, 156.5. HRMS (ESI) *m/z*: $[M + H]^+$ Calcd for $C_{36}H_{38}N_2O_3$ 547.2961; Found 547.2958.

14,18-Diethyl-6,21-dihydro-6-hydroxy-2,21-dimethoxy-13,19-dimethyl-23-carbabenzo[*h*]benziporphyrin (**39a**). Further elution of the first column from the previous reaction with 50:50 dichloromethane-chloroform gave a second deep purple band. The solution was evaporated and dried overnight in vacuo to give the hydroxy-derivative (1.6 mg, 0.0030 mmol, 6.8%) as a purple film. UV-Vis (CH_2Cl_2): λ_{max}/nm (relative intensity) 342 (1.00), 551 (sh, 0.91), 579 (0.99). ^1H NMR (500 MHz, $CDCl_3$): δ 1.11 (3H, t, *J* = 7.6 Hz), 1.16 (3H, t, *J* = 7.6 Hz) (2 x CH_2CH_3), 2.13 (3H, s, 13-Me), 2.21 (3H, s, 19-Me), 2.53-2.61 (4H, m, 14,18-CH_2), 3.43 (3H, s, 21-OMe), 3.75 (3H, s, 2-OMe), 5.73 (1H, br s), 5.74 (1H, br s) (6,21-H), 6.67 (1H, s, 16-H), 6.77 (1H, d, *J* = 8.2 Hz, 3-H), 6.93 (1H, br s, 23-H), 7.15 (1H, t, *J* = 0.7 Hz, 11-H), 7.22-7.27 (2H, m. 4,9^2-H), 7.31 (1H, dt, *J* = 1.1, 7.5 Hz, 8^2-H), 7.67 (1H, ddd, *J* = 0.7, 1.1, 7.4 Hz, 9^1-H), 7.74 (1H, ddd, *J* = 0.7, 1.1, 7.4 Hz, 8^1-H), 8.22 (1H, d, *J* = 2.1 Hz, 22-H), 11.16 (1H, br s, NH). ^1H NMR (500 MHz, C_6D_6): δ 0.97 (3H, t, *J* = 7.6 Hz), 1.07 (3H, t, *J* = 7.6 Hz) (2 x CH_2CH_3), 1.82 (3H, s, 13-Me), 2.19 (3H, s, 19-Me), 2.31 (2H, q, *J* = 7.6 Hz), 2.45 (2H, q, *J* = 7.6 Hz) (2 x CH_2CH_3), 3.19 (3H, s, 2-OMe), 3.26 (3H, s, 21-OMe), 5.61 (1H, s, 6-H), 5.87 (1H, s, 21-H), 6.32 (1H, d, *J* = 8.1 Hz, 3-H), 6.67 (1H, s, 16-H), 6.97 (1H, dd, *J* = 2.2, 8.1 Hz, 4-H), 7.13 (1H, s, 11-H), 7.18-7.21 (1H, m, 8^2 or 9^2-H), 7.28 (1H, br s, 23-H), 7.30-7.33 (1H, m, 8^2 or 9^2-H), 7.57 (1H, d, *J* = 7.5 Hz, 9^1-H), 7.88 (1H, d, *J* = 7.5 Hz, 8^1-H), 8.51 (1H, br s, 22-H), 11.55

(1H, v br, NH). ^{1}H NMR (500 MHz, *d*$_6$-DMSO): δ 1.07 (3H, t, *J* = 7.5 Hz), 1.12 (3H, t, *J* = 7.5 Hz) (2 x CH_2CH_3), 2.13 (3H, s), 2.18 (3H, s) (13.19-Me), 2.55-2.65 (4H, m, 2 x CH_2CH_3), 3.33 (3H, s), 3.71 (3H, s) (2,21-OMe), 5.57 (1H, d, *J* = 6.4 Hz, 6-H), 5.67 (1H, d, *J* = 6.4 Hz, OH), 5.68 (1H, s, 21-H), 6.69 (1H, br s), 6.83 (1H, s), 6.87 (1H, d, *J* = 8.1 Hz, 3-H), 7.21 (1H, dt, *J* = 0.8, 7.5 Hz), 7.258 (1H, dd, *J* = 2.2, 8.2 Hz, 4-H), 7.263 (1H, s), 7.29 (1H, dt, *J* = 0.8, 7.5 Hz), 7.67 (1H, d, *J* = 7.4 Hz), 7.85 (1H, d, *J* = 7.4 Hz), 8.04 (1H, d, *J* = 2.0 Hz, 22-H), 11.03 (1H, br s, NH). ^{13}C{^{1}H} NMR (125 MHz, $CDCl_3$): δ 9.5 (19-Me), 9.6 (13-Me), 16.38, 16.46, 17.9, 18.3, 55.7 (2-OMe), 57.6 (21-OMe), 71.5 (CH-O), 72.2 (CH-O), 109.9 (3-CH), 116.1 (11-CH), 116.5 (16-CH), 119.4 (9^1-CH), 120.9 (8^1-CH), 125.4 (9^2-CH), 126.3 (22-CH), 126.8 (23-CH), 127.2, 127.4 (8^2-CH), 127.6 (4-CH), 128.4, 131.0, 134.1, 137.2, 139.0, 139.1, 139.8, 141.2, 141.9, 142.7, 148.2, 156.3. HRMS (ESI) *m/z*: $[M + H]^+$ Calcd for $C_{35}H_{37}N_2O_3$ 533.2804; Found 533.2798.

14,18-Diethyl-6,21-dihydro-2,4,6,21-tetramethoxy-13,19-dimethyl-23-carbabenzo[*h*]benziporphyrin (**38b**). Dimethoxycarbabenziporphyrin **12d** (17.0 mg, 0.033 mmol) was reacted with silver acetate under the foregoing conditions to give the tetramethoxyporphyrinoid (6.6 mg, 0.0114 mmol, 34%) as a dark purple solid, mp >260 ºC. UV-Vis (CH_2Cl_2): λ_{max}/nm ($\log_{10}$ ε) 341 (4.37), 550 (sh, 4.31), 579 (4.35). ^{1}H NMR (500 MHz, $CDCl_3$): δ 1.10 (3H, t, *J* = 7.5 Hz), 1.15 (3H, t, *J* = 7.5 Hz) (2 x CH_2CH_3), 2.12 (3H, s, 13-Me), 2.19 (3H, s, 19-Me), 2.52-2.61 (4H, m, 14,18-CH_2), 3.39 (3H, s, 21-OMe), 3.42 (3H, s, 6-OMe), 3.77 (3H, s, 2-OMe), 3.78 (3H, s, 4-OMe), 5.68 (1H, d, *J* = 0.6 Hz, 21-H), 5.90 (1H, br dd, *J* = 0.6, 1.4 Hz, 6-H), 6.44 (1H, s, 3-H), 6.67 (1H, s, 16-H), 6.99 (1H, br s, 23-H), 7.12 (1H, t, *J* = 0.7 Hz, 11-H), 7.20 (1H, dt, *J* = 1.1, 7.5 Hz, 9^2-H), 7.29 (1H, dt, *J* = 1.1, 7.4 Hz, 8^2-H), 7.62 (1H, dt, *J* = 0.8, 7.4 Hz, 8^1-H), 7.64 (1H, dt, *J* = 0.9, 7.4 Hz, 9^1-H), 8.09 (1H, d, *J* = 0.6 Hz, 22-H), 11.22

(1H, br s, NH). $^{13}C\{^{1}H\}$ NMR (125 MHz, $CDCl_3$): δ 9.5 (19-Me), 9.6 (13-Me), 16.4, 16.5, 17.9, 18.3, 55.7 (OMe), 56.2 (OMe), 56.3 (OMe), 57.3 (21-OMe), 71.1 (6-CH), 71.8 (21-CH), 95.3 (3-CH), 115.6 (11-CH), 116.4 (16-CH), 119.0, 119.2 (9^1-CH), 120.8 (8^1-CH), 122.4, 125.1 (9^2-CH), 126.4, 127.1 (23-CH), 127.4 (8^2-CH), 128.3, 128.4 (22-CH), 137.9, 139.1, 139.6, 140.1, 140.9, 142.0, 142.2, 147.5, 156.8, 158.4. HRMS (ESI) *m/z*: $[M + H]^+$ Calcd for $C_{37}H_{41}N_2O_4$ 577.3066; Found 577.3069.

14,18-Diethyl-6,21-dihydro-6-hydroxy-2,4,21-trimethoxy-13,19-dimethyl-23-carbabenzo[*h*]benziporphyrin (**39b**). Further elution of the first column from the previous reaction with 50:50 dichloromethane-chloroform gave a deep purple band. The solution was evaporated and dried overnight in vacuo to give the hydroxy-derivative (1.2 mg, 0.0021 mmol, 6.5%) as a purple film. UV-Vis (CH_2Cl_2): λ_{max}/nm (relative intensity) 342 (1.00), 550 (sh, 0.87), 580 (0.96). ^{1}H NMR (500 MHz, $CDCl_3$): δ 1.11 (3H, t, *J* = 7.6 Hz), 1.15 (3H, t, *J* = 7.6 Hz) (2 x CH_2CH_3), 2.13 (3H, s, 13-Me), 2.19 (3H, s, 19-Me), 2.53-2.61 (4H, m, 14,18-CH_2), 3.41 (3H, s, 21-OMe), 3.77 (3H, s), 3.79 (3H, s) (2,4-OMe), 5.69 (1H, s, 21-H), 6.35 (1H, br s, 6-H), 6.43 (1H, s, 3-H), 6.68 (1H, s, 16-H), 6.99 (1H, br s, 23-H), 7.14 (1H, t, *J* = 0.7 Hz, 11-H), 7.22 (1H, dt, *J* = 1.0, 7.5 Hz, 9^2-H), 7.31 (1H, dt, *J* = 1.0, 7.5 Hz, 8^2-H), 7.67 (1H, dt, *J* = 0.9, 7.5 Hz, 9^1-H), 7.76 (1H, dt, *J* = 0.9, 7.4 Hz, 8^1-H), 8.10 (1H, s, 22-H), 10.91 (1H, br s, NH). ^{1}H NMR (500 MHz, C_6D_6): δ 0.97 (3H, t, *J* = 7.6 Hz), 1.10 (3H, t, *J* = 7.6 Hz) (2 x CH_2CH_3), 1.80 (3H, s, 13-Me), 2.23 (3H, s, 19-Me), 2.32 (2H, q, *J* = 7.6 Hz), 2.48 (2H, q, *J* = 7.6 Hz) (14,18-CH_2), 3.19 (3H, s), 3.20 (3H, s), 3.30 (3H, s) (3 x OMe), 5.89 (1H, s), 5.98 (1H, s) (6,21-H), 6.64 (1H, br s), 6.72 (1H, s), 7.11 (1H, s), 7.15-7.26 (2H, m, 8^2,9^2-H, 7.42 (1H, s), 7.54 (1H, d, *J* = 7.4 Hz), 7.89 (1H, d, *J* = 7.4 Hz) (8^1,9^1-H), 8.45 (1H, s, 22-H), 11.15 (1H, v br, NH). ^{1}H NMR (500 MHz, *d*$_6$-DMSO): δ 1.05 (3H, t, *J* = 7.5 Hz), 1.09 (3H, t, *J* = 7.5 Hz) (2 x CH_2CH_3), 2.12 (3H, s), 2.16

(3H, s) (13,19-Me), 2.55-2.64 (4H, m, 14,18-CH_2), 3.30 (3H, s, 21-OMe), 3.74 (3H, s), 3.76 (3H, s) (2,4-OMe), 5.60 (1H, s, 21-H), 5.63 (1H, d, J = 6.9 Hz, OH), 6.04 (1H, d, J = 6.9 Hz, 6-H), 6.61 (1H, s), 6.72 (1H, br s), 6.84 (1H, s), 7.20-7.23 (1H, m), 7.27 (1H, s), 7.27-7.30 (1H, m), 7.63 (1H, d, J = 7.4 Hz), 7.87 (1H, d, J = 7.4 Hz), 7.91 (1H, s), 10.94 (1H, br s, NH). $^{13}C\{^1H\}$ NMR (125 MHz, $CDCl_3$): δ 9.5 (19-Me), 9.6 (13-Me), 16.4, 16.5, 18.0, 18.3, 55.8 (Ar-OMe), 56.2 (Ar-OMe), 57.5 (21-OMe), 63.0 (6-CH), 71.8 (21-CH), 95.5 (3-CH), 115.9 (11-CH), 116.5 (16-CH), 119.3 (9^1-CH), 121.1 (8^1-CH), 122.1, 122.4, 125.3 (9^2-CH), 126.5 (23-CH), 126.6, 127.5 (8^2-CH and 22-CH), 128.4, 137.6, 139.2, 140.1, 141.6, 142.4, 148.5, 156.7, 156.9. HRMS (ESI) *m/z*: $[M + H]^+$ Calcd for $C_{36}H_{39}N_2O_4$ 563.2910; Found 563.2907.

6,21-Dihydro-2,4,6,21-tetramethoxy-14,18-bis(2-methoxycarbonylethyl)-13,19-dimethyl-23-carbabenzo[*h*]benziporphyrin (**38c**). Dimethoxycarbabenziporphyrin **12f** (20.0 mg, 0.029 mmol) was reacted with silver(I) acetate under the conditions used to prepare **38a**. The product fraction was purified on a grade 3 alumina column, eluting with dichloromethane, and recrystallized from chloroform-hexanes to give **38c** (8.5 mg, 0.0122 mmol, 42%) as a dark sold, mp 233-234 °C. UV-Vis (CH_2Cl_2): λ_{max}/nm ($\log_{10}$ ε) 340 (4.33), 547 (sh, 4.30), 576 (4.35). ^1H NMR (500 MHz, $CDCl_3$): δ 2.13 (3H, s, 13-Me), 2.21 (3H, s, 19-Me), 2.49 (2H, t, J = 7.6 Hz, 14-$CH_2C\mathit{H}_2CO$), 2.54 (2H, t, J = 7.8 Hz, 18-$CH_2C\mathit{H}_2CO$), 2.88 (2H, t, J = 7.6 Hz, 14-CH_2), 2.90 (2H, m, 18-CH_2), 3.38 (3H, s, 21-OMe), 3.41 (3H, s, 6-OMe), 3.64 (3H, s), 3.67 (3H, s) (2 x ester OMe), 3.77 (3H, s), 3.79 (3H, s) (2,4-OMe), 5.67 (1H, s, 21-H), 5.89 (1H, br s, 6-H), 6.44 (1H, s, 3-H), 6.77 (1H, s, 16-H), 6.95 (1H, br s, 23-H), 7.09 (1H, br t, J = 1.0 Hz, 11-H), 7.20 (1H, dt, J = 1.0, 7.5 Hz, 9^2-H), 7.29 (1H, dt, J = 1.0, 7.4 Hz, 8^2-H), 7.61 (1H, d, J = 7.4 Hz, 8^1-H), 7.63 (1H, d, J = 7.4 Hz, 9^1-H), 8.07 (1H, s, 22-H), 11.08 (1H, br s, NH). $^{13}C\{^1H\}$ NMR (125 MHz, $CDCl_3$): δ 9.6 (19-Me), 9.8 (13-Me), 19.9 (14-CH_2), 20.2 (18-CH_2), 35.5 (CH_2CO), 35.7

(CH_2CO), 51.86 (ester OMe), 51.87 (ester OMe), 55.7 (Ar-OMe), 56.2 (Ar-OMe and 6-OMe), 57.3 (21-OMe), 71.0 (6-CH), 71.6 (21-CH), 95.2 (3-CH), 115.4 (11-CH), 117.1 (16-CH), 118.8, 119.2 (9^1-CH), 120.9 (8^1-CH), 122.1, 125.3 (9^2-CH), 126.9 (23-CH), 127.2, 127.6 (8^2-CH), 128.3 (22-CH), 129.3, 136.5, 138.0, 138.4, 139.0, 139.9, 140.6, 142.0, 147.9, 156.8, 158.4, 173.3 (C=O), 173.4 (C=O). HRMS (ESI) *m/z*: $[M + H]^+$ Calcd for $C_{41}H_{45}N_2O_8$ 693.3176; Found 693.3175.

Computational Studies. All calculations were performed using Gaussian 09 Rev D.01 running on a Linux-based computer.[46] Geometry optimization and frequency calculations of the *adj*-dicarbaporphyrinoid systems were performed at the density functional theory (DFT) level of theory with the B3LYP functional and the 6-311++G(d,p) triple-ζ basis set.[47-50] Single-point energy calculations were performed on the minimized structures using both the B3LYP-D3[51] and M06-2X[52] functionals with a 6-311++G(d,p) triple-ζ basis set. The resulting Cartesian coordinates of the molecules can be found in Supporting Information.

Two types of NMR calculations were performed: the GIAO method was used to obtain NICS values,[53] and CGST to obtain AICD plots.[45,54] NICS(0) was calculated at the mean position of all four heavy atoms in the middle of the macrocycle. NICS(a), NICS(b), NICS(c), NICS(d), and NICS(e) values were obtained by applying the same method to the mean position of the heavy atoms that comprise the individual rings of each macrocycle. In addition, $NICS(1)_{zz}$, $NICS(1a)_{zz}$, $NICS(1b)_{zz}$, $NICS(1c)_{zz}$, $NICS(1d)_{zz}$, and $NICS(1e)_{zz}$ were obtained by applying the same method to ghost atoms placed 1 Å above each of the corresponding NICS(0) points and extracting the zz contribution of the magnetic tensor. AICD for all the compounds were plotted, and these plots can also be found in Supporting Information.

ASSOCIATED CONTENT

Supporting Information

The Supporting Information is available free of charge on the ACS Publications website.

Tables giving Cartesian coordinates, calculated energies, selected bond lengths and AICD plots, and selected UV-Vis, ^{1}H NMR, ^{1}H-^{1}H COSY, HSQC, DEPT-135, ^{13}C NMR, and mass spectra are provided (pdf).

AUTHOR INFORMATION

Corresponding Author

*E-mail: tdlash@ilstu.edu

ORCID

Timothy D. Lash: 0000-0002-0050-0385

Deyaa I. AbuSalim: 0000-0003-0813-0486

Notes

The authors declare no competing financial interest.

ACKNOWLEDGMENTS

This work was supported by the National Science Foundation under grant no. CHE-1465049, and the Petroleum Research Fund, administered by the American Chemical Society.

References

(1) Lash, T. D. Carbaporphyrinoid Systems. *Chem. Rev.* **2017**, *117*, 2313−2446.

(2) Toganoh, M.; Furuta, H. Synthesis and Metal Coordination of N-Confused and N-Fused

Porphyrinoids. In *Handbook of Porphyrin Science − With Applications to Chemistry, Physics, Material Science, Engineering, Biology and Medicine*; Kadish, K. M.; Smith, K. M.; Guilard, R., Eds.; World Scientific Publishing: Singapore, 2010; Vol. 2, pp 295−367.

(3) Toganoh, M.; Furuta, H. Blooming of Confused Porphyrinoids − Fusion, Expansion, Contractions, and More Confusion. *Chem. Commun.* **2012**, *48*, 937−954.

(4) Li, D.; Lash, T. D. Synthesis and Reactivity of Carbachlorins and Carbaporphyrins. *J. Org. Chem.* **2014**, *79*, 7112−7121.

(5) Sahota, N.; Ferrence, G. M.; Lash, T. D. Synthesis and Properties of Carbaporphyrin and Carbachlorin Dimethyl Esters Derived from Cyclopentanedialdehydes. *J. Org. Chem.* **2017**, *82*, 9715−9730.

(6) Lash, T. D.; Hayes, M. J. Carbaporphyrins. *Angew. Chem., Int. Ed. Engl.* **1997**, *36*, 840−842.

(7) Lash, T. D. Out of the Blue! Azuliporphyrins and Related Carbaporphyrinoid Systems. *Acc. Chem. Res.* **2016**, *49*, 471−482.

(8) Bergman, K. M.; Ferrence, G. M.; Lash, T. D. Tropiporphyrins, Cycloheptatrienyl Analogues of the Porphyrins: Synthesis, Spectroscopy, Chemistry and Structural Characterization of a Silver(III) Derivative. *J. Org. Chem.* **2004**, *69*, 7888−7897.

(9) Lash, T. D. Benziporphyrins, a Unique Platform for Exploring the Aromatic Characteristics of Porphyrinoid Systems. *Org. Biomol. Chem.* **2015**, *13*, 7846−7878.

(10) Lash, T. D. Metal Complexes of Carbaporphyrinoid Systems. *Chem. - Asian J.* **2014**, *9*, 682−705.

(11) Richter, D. T.; Lash, T. D. Conjugated Macrocycles Related to the Porphyrins. Part 18. Synthesis and Spectroscopic Characterization of Electron-rich Benzi- and

Oxybenziporphyrins: Influence of Steric and Electronic Factors on Porphyrinoid Aromaticity. *Tetrahedron* **2001**, *57*, 3657−3671.

(12) Lash, T. D.; Szymanski, J. T.; Ferrence, G. M. Tetraaryldimethoxybenziporphyrins. At the Edge of Carbaporphyrinoid Aromaticity. *J. Org. Chem.* **2007**, *72*, 6481−6492.

(13) AbuSalim, D. I.; Lash, T. D. Relative Stability of Benziporphyrin and Naphthiporphyrin Tautomers and the Emergence of Macrocyclic Diatropicity. *Org. Biomol. Chem.* **2014**, *12*, 8719−8736.

(14) (a) Furuta, H.; Maeda, H.; Osuka, A. Doubly N-Confused Porphyrin: A New Complexing Agent Capable of Stabilizing Higher Oxidation States. *J. Am. Chem. Soc.* **2000**, *122*, 803−807. (b) Maeda, H.; Osuka, A.; Furuta, H. Trans Doubly N-Confused Porphyrins: Cu(III) Complexation and Formation of Rodlike Hydrogen-Bonding Networks. *J. Am. Chem. Soc.* **2003**, *125*, 15690−15691.

(15) Lash, T. D.; Romanic, J. L.; Hayes, M. J.; Spence, J. D. Towards Hydrocarbon Analogues of the Porphyrins: Synthesis and Spectroscopic Characterization of the First Dicarbaporphyrin. *Chem. Commun.* **1999**, *35*, 819−820.

(16) AbuSalim, D. I.; Ferrence, G. M.; Lash, T. D. Synthesis of an *adj*-Dicarbaporphyrin and the Formation of an Unprecedented Tripalladium Sandwich Complex. *J. Am. Chem. Soc.* **2014**, *136*, 6763−6772.

(17) (a) Lash, T. D.; Lammer, A. D.; Ferrence, G. M. Two-step Synthesis of Stable Dioxadicarbaporphyrins from Bis(3-indenyl)methane. *Angew. Chem., Int. Ed.* **2012**, *51*, 10871−10875. (b) Lash, T. D.; Fosu, S. C.; Smolczyk, T. J.; AbuSalim, D. I. Synthesis of Expanded Porphyrinoids with Azulene and Indene Subunuits and an *opp*-Dioxadicarbaporphyrin from Fulvene Carbinols and a Dioxacarbatripyrrin. *J. Org. Chem.*

2018, *83*, 12619-12631.

(18) Lash, T. D.; AbuSalim, D. I.; Ferrence, G. M. *adj*-Dicarbachlorin, the First Example of a Free Base Carbaporphyrinoid System with an Internal Methylene Unit. *Chem. Commun.* **2015**, *51*, 15952-15955.

(19) Zhang, Z.; Ferrence, G. M.; Lash, T. D. *adj*-Diazuliporphyrins, a New Family of Dicarbaporphyrinoids with Unprecedented Mesoionic Characteristics. *Org. Lett.* **2009**, *11*, 101−104.

(20) (a) Sprutta, N.; Swiderska, M.; Latos-Grazynski, L. Dithiadiazuliporphyrin: Facile Generation of Carbaporphyrinoid Cation Radical and Dication. *J. Am. Chem. Soc.* **2005**, *127*, 13108−13109. (b) Sprutta, N.; Siczek, M.; Latos-Grazynski, L.; Pawlicki, M.; Szterenberg, L.; Lis, T. Dioxadiazuliporphyrin: A Near-IR Redox Switchable Chromophore. *J. Org. Chem.* **2007**, *72*, 9501−9509.

(21) Fosu, S. C.; Ferrence, G. M.; Lash, T. D. Synthesis and Metalation of Dimethoxybenziporphyrins, Thiabenziporphyrins and Dibenziporphyrins. *J. Org. Chem.* **2014**, *79*, 11061−11074.

(22) Graham, S. R.; Colby, D. A.; Lash, T. D. Azulene Analogues of Tripyrranes and Carbaporphyrinoids Therefrom. *Angew. Chem., Int. Ed.* **2002**, *41*, 1371−1374.

(23) Lash, T. D.; Lammer, A. D.; Idate, A. S.; Colby, D. A.; White, K. Preparation of Azulene-Derived Fulvenedialdehydes and their Application to the Synthesis of Stable *adj*-Dicarbaporphyrinoids. *J. Org. Chem.* **2012**, *77*, 2368−2381.

(24) Xu, L.; Lash, T. D. Synthesis of Aromatic Dicarbaporphyrinoids from Resorcinol and 2-Methylresorcinol. *Tetrahedron Lett.* **2006**, *47*, 8863-8866.

(25) Szyszko, B.; Bialonska, A.; Szterenberg, L.; Latos-Grazyński, L. Phenanthriporphyrin:

Antiaromatic Aceneporphyrinoid as Surrounding for Hypervalent Organophosphorus(V). *Angew. Chem., Int. Ed.* **2015**, *54*, 4932−4936.

(26) Kupietz, Kl; Bialek, M. J.; Bialonska, A.; Szyszko, B.; Latos-Grazyński, L. Organocopper(III) Phenanthriporphyrin-Exocyclic Transformations. *Inorg. Chem.* **2019**, *58*, 1451-1461

(27) (a) Ke, X.-S.; Hong, Y.; Tu, P.; He, Q.; Lynch, V. M.; Kim, D.; Sessler, J. L. Hetero Cu(III)-Pd(II) Complex of a Dibenzo[*g,p*]chrysene-Fused Bis-dicarbacorrole with Stable Organic Radical Character. *J. Am. Chem. Soc.* **2017**, *139*, 15232-15238. (b) Ke, X.-S.; Hong, Y.; Lynch, V. M.; Kim, D.; Sessler, J. L. Metal-Stabilized Quinoidal Dibenzo[*g, p*]chrysene-Fused Bis-dicarbacorrole System. *J. Am. Chem. Soc.* **2018**, *140*, 7579-7586.

(28) Lash, T. D. What's in a Name? The MacDonald Condensation. *J. Porphyrins Phthalocyanines* **2016**, *20*, 855−888.

(29) (a) Jackson, A. H.; Pandey, R. K.; Smith, K. M. Synthetic and Biosynthetic Studies of Porphyrins. Part 10. Syntheses of Porphyrins with Acetic, Propionic, and Butyric Acid Side-Chains for Biosynthetic Studies. *J. Chem. Soc., Perkin Trans. 1* **1987**, *1987*, 299-305. (b) Lash, T. D.; Armiger, Y. L. S.-T. Conjugated Macrocycles Related to the Porphyrins. Part 2. Further Synthetic and Spectroscopic Studies on Difuryl Analogs of the Oxophlorins. *J. Heterocyclic Chem.* **1991**, *28*, 965-970.

(30) Arnold, Z. Synthetic Reactions of Dimethylformamide. XXII. Formation and Preparation of Formyl Derivatives of Indene. *Collect. Czech. Chem. Commun.* **1965**, *30*, 2783−2792.

(31) Lash, T. D.; Colby, D. A.; Idate, A. S.; Davis, R. N. Fulvene Dialdehyde Strategy for *adj*-Dicarbaporphyrinoid Synthesis: Preparation of a 22-Carbaazuliporphyrin. *J. Am. Chem. Soc.* **2007**, *129*, 13800-13801.

(32) Davis, R. N.; Lash, T. D. Formation of Stable Fulvene and Difulvene Aldehydes from Benzaldehydes and an Indene-Derived Enamine: Preparation of Novel Indene Fused Benzodiazepines and Attempted Syntheses of Di- and Tricarbaporphyrinoid Systems. *Tetrahedron* **2009**, *65*, 9935-9943.

(33) Hathaway, B. A.; White, K. L.; McGill, M. E. Comparison of Iodination of Methoxylated Benzaldehydes and Related Compounds using Iodine/Silver Nitrate and Iodine/Periodic Acid. *Synth. Commun.* **2007**, *37*, 3855-3860.

(34) Iida, T.; Wada, T.; Tomimoto, K.; Mase, T. Tributylmagnesium ate Complex-Mediated Novel Bromine–Magnesium Exchange Reaction for Selective Monosubstitution of Dibromoarenes. *Tetrahedron Lett.* **2001**, *42*, 4841-4844.

(35) Ito, S.; Kubo, T.; Morita, N.; Matsui, Y.; Watanabe, T.; Ohta, A.; Fujimori, K.; Murafuji, T.; Sugihara, Y.; Tajiri, A. Preparation of Azulenyllithium and Magnesium Reagents Utilizing Halogen–Metal Exchange Reaction of Several Iodoazulenes with Organolithium or Magnesium ate Complex. *Tetrahedron Lett.* **2004**, *45*, 2891-2894.

(36) Seitz, L. M.; Brown, T. L. Organometallic Exchange Reactions. III. Lithium-7 and Proton Nuclear Magnetic Resonance Spectra of Methyllithium-Dimethylmagnesium and Methyllithium-Dimethylzinc in Ether. *J. Am. Chem. Soc.* **1996**, *88*, 4140–4147.

(37) Dumouchel, S.; Mongin, F.; Trécourt, F.; Quéguiner, G. Synthesis and Reactivity of Lithium Tri(quinolinyl)magnesates. *Tetrahedron* **2003**, *59*, 8629–8640.

(38) Hatano, M.; Matsumura, T.; Ishihara, K. Highly Alkyl-Selective Addition to Ketones with Magnesium Ate Complexes Derived from Grignard Reagents. *Org. Lett.* **2005**, *7*, 573–576.

(39) Inoue, A.; Kitagawa, K.; Shinokubo, H.; Oshima, K. Selective Halogen−Magnesium Exchange Reaction via Organomagnesium Ate Complex. *J. Org. Chem.* **2001**, *66*, 4333–

4339.

(40) Jain, P.; Ferrence, G. M.; Lash, T. D. Preparation of Furan and Thiophene-Derived Fulvene Dialdehydes: Synthesis and Structural Characterization of a 22-Oxa-21-carbaporphyrin and a Related Palladium(II) Organometallic Complex. *J. Org. Chem.* **2010**, *75*, 6563−6573.

(41) (a) Ghosh, A. First-principles Quantum Chemical Studies of Porphyrins. *Acc. Chem. Res.* **1998**, *31*, 189−198. (b) Ghosh, A. Quantum Chemical Studies of Molecular Structures and Potential Energy Surfaces of Porphyrins and Hemes. *The Porphyrin Handbook*; Kadish, K. M.; Smith, K. M.; Guilard, R., Eds.; Academic Press: San Diego, 2000; Vol. 7, pp 1−38.

(42) Alonso, M.; Geerlings, P.; De Proft, F. Exploring the Structure- Aromaticity Relationship in Hückel and Möbius N-Fused Pentaphyrins using DFT. *Phys. Chem. Chem. Phys.* **2014**, *16*, 14396−14407.

(43) Alonso, M.; Geerlings, P.; De Proft, F. Topology Switching in [32]Heptaphyrins Controlled by Solvent, Protonation, and *meso* Substituents. *Chem. - Eur. J.* **2013**, *19*, 1617−1628.

(44) Schleyer, P. v. R.; Maerker, C.; Dransfeld, A.; Jiao, H.; van Eikema Hommes, N. J. R. Nucleus-Independent Chemical Shifts: a Simple and Efficient Aromaticity Probe. *J. Am. Chem. Soc.* **1996**, *118*, 6317−6318.

(45) Geuenich, D.; Hess, K.; Köhler, F.; Herges, R. Anisotropy of Induced Current Density (ACID), a General Method to Quantify and Visualize Electronic Delocalization. *Chem. Rev.* **2005**, *105*, 3758− 3772.

(46) Frisch, M. J.; Trucks, G. W.; Schlegel, H. B.; Scuseria, G. E.; Robb, M. A.; Cheeseman, J. R.; Scalmani, G.; Barone, V.; Petersson, G. A.; Nakatsuji, H.; et al. *Gaussian 09, Revision D.01*; Gaussian, Inc., Wallingford, CT, 2016.

(47) Becke, A. D. Density Functional Thermochemistry. III. The Exact Role of Exchange. *J. Chem. Phys.* **1993**, *98*, 5648−5652.

(48) Lee, C.; Yang, W.; Parr, R. G. Development of the Colle- Solvetti Correlation-Energy Formula into a Functional of the Electron Density. *Phys. Rev. B: Condens. Matter Mater. Phys.* **1988**, *37*, 785− 789.

(49) Vosko, S. H.; Wilk, L.; Nusair, M. Accurate Spin-Dependent Electron Liquid Correlation Energies for Local Spin Density Calculations: a Critical Analysis. *Can. J. Phys.* **1980**, *58*, 1200−1211.

(50) Stephens, P. J.; Devlin, F. J.; Chabalowski, C. F.; Frisch, M. J. *Ab Initio* Calculations of Vibrational Absorption and Circular Dichroism Spectra using Density Functional Force Fields. *J. Phys. Chem.* **1994**, *98*, 11623−11627.

(51) Grimme, S.; Antony, J.; Ehrlich, S.; Krieg, H. A Consistent and Accurate Ab Initio Parametrization of Density Functional Dispersion Correction (DFT-D) for the 94 Elements H-Pu. *J. Chem. Phys.* **2010**, *132*, 154104-1−154104-19.

(52) Zhao, Y.; Truhlar, D. G. The M06 Suite of Density Functionals for Main Group Thermochemistry, Thermochemical Kinetics, Noncovalent Interactions, Excited States, and Transition Elements: Two New Functionals and Systematic Testing of Four M06-Class Functionals and 12 Other Functionals. *Theor. Chem. Acc.* **2008**, *120*, 215−241.

(53) Wolinski, K.; Hinton, J. F.; Pulay, P. Efficient Implementation of the Gauge-independent Atomic Orbital Method for NMR Chemical Shift Calculations. *J. Am. Chem. Soc.* **1990**, *112*, 8251−8260.

(54) Herges, R.; Geuenich, D. Delocalization of Electrons in Molecules. *J. Phys. Chem. A* **2001**, *105*, 3214−3220.